TEMPORAL ANALYSIS OF GAMMA-RAY BURST 190114C USING DATA FROM THE FERMI GAMMA-RAY SPACE TELESCOPE

by

Urooj Murtaza

Supervisor
Dr. Saeeda Sajjad

Department of Space Sciences
Institute of Space Technology, Islamabad

2020

TEMPORAL ANALYSIS OF GAMMA-RAY BURST 190114C USING DATA FROM THE FERMI GAMMA-RAY SPACE TELESCOPE

A thesis submitted to
Institute of Space Technology
in partial fulfillment of the requirements
for the degree of Bachelor of Science in
Space Sciences

by

Urooj Murtaza

Supervisor

Dr. Saeeda Sajjad

Department of Space Sciences
Institute of Space Technology, Islamabad
2020

Institute of Space Technology

Department of Space Sciences

TEMPORAL ANALYSIS OF GAMMA-RAY BURST 190114C USING DATA FROM THE FERMI GAMMA-RAY SPACE TELESCOPE

by

Urooj Murtaza

APPROVAL BY BOARD OF EXAMINERS

Dr. Saeeda Sajjad

AUTHOR'S DECLARATION

I take full responsibility of the research work conducted during the FYP, BS Thesis titled "Temporal analysis of Gamma-Ray Burst 190114C using data from the Fermi Gamma-Ray Space Telescope".

I solemnly declare that the research and development work presented in the FYP, BS Thesis is done solely by me with no significant help from any other person; however, small help wherever taken is duly acknowledged. I have also written the complete thesis by myself. Moreover, I have not presented this thesis (or substantially similar research and development work) or any part of the thesis previously to any other degree awarding institution within Pakistan or abroad.

I understand that the management of IST has a zero tolerance policy towards plagiarism. Therefore, I as an author of the above-mentioned thesis, solemnly declare that no portion of my thesis has been plagiarized and any material used in the thesis from other sources is properly referenced. Moreover, the thesis does not contain any literal citing (verbatim) of more than 70 words (total) even by giving a reference unless I have obtained the written permission of the publisher to do so. Furthermore, the work presented in the thesis is my own original work and I have positively cited the related work of the other researchers by clearly differentiating my work from their relevant

work.

I further understand that if I am found guilty of any form of plagiarism in my thesis work even after my graduation, the Institute reserves the right to revoke my MS degree. Moreover, the Institute will also have the right to publish my name on its website that keeps a record of the students who plagiarized in their thesis work.

_____

Urooj Murtaza

160601002

I hereby acknowledge that submitted thesis is final version and should be scrutinized for plagiarism as per IST policy.

_____

Dr Saeeda Sajjad

Dated: _____

_____

Verified by Plagiarism Cell Officer

Dated: _____

DEDICATION

To my parents and teachers.

ABSTRACT

Gamma-Ray Bursts (GRBs) are one of the highest energy events in the universe but little is known about them. The sources and the mechanisms of emission have been studied for many years but are still not very clearly understood. The temporal profiles of Gamma-Ray Burst can provide clues about the very nature of GRBs. In this project we aimed to find the temporal characteristics of the Gamma-Ray Burst 190114C which is a recently detected GRB in the Tera-electron Volt (TeV) energy range. The temporal profile of this GRB hasn't been studied in detail as of now. For our analysis we have used data from the Fermi Gamma-Ray Space Telescope, have utilized softwares like Rmfit for background-fitting and Pyroot along with Norris-2005 temporal model for curve-fitting procedures. The time evolution of the GRB 190141C suggested that width of a pulse increases and amplitude decreases with time. We also got an inverse relationship between the rise and fall duration of a pulse and no correlation between the pulse width and asymmetry. These results where in agreement with the results observed by J.P Norris [1].

Table of Contents

List of Figures

1. INTRODUCTION

Gamma rays are the most energetic forms of electromagnetic radiation released during processes like radioactive decay, nuclear fusion, synchrotron radiation etc [1]. Gamma-Ray Bursts (GRBs) are intense and focused emissions of Gamma rays followed by low energy electromagnetic radiation [2]. A Gamma-Ray Burst emission can be divided into two main phases, the prompt emission and the afterglow. For our analysis we will be working on the Prompt emission phase which lasts for a few seconds to minutes. We will be using data from the 4 NAI detectors within GBM which is a complementary instrument onboard the Fermi telescope.

Our study aims to understand the pulse properties of the GRB 190114C which has a T90 duration of 117 seconds making it a long GRB with energy reaching up to 0.2 to 1 Tera-electron Volt making it a VHE (very high energy) GRB [3]. The red-shift of this GRB is 0.4245 [2]. The name of this GRB has been given to it based on the date on which it was detected which is 14th of January 2019 where the "C" indicates that it was the 3rd GRB to be observed on that date. A detailed temporal analysis of this GRB has not been done yet which makes our study very important towards understanding this GRB. The temporal analysis of this GRB is vital in a way that can provide us with clues about high energy phenomena and how Gamma-Ray Burst emissions progress with time. We might also be able to confirm some long standing concepts about long GRBs.

We will use tools like Rmfit for background fitting and pyroot along with the Norris-2005 model for curve-fitting for our analysis of the pulses of this GRB. GRB pulses are superimposed on each other in a GRB signal with

[1] https://heasarc.gsfc.nasa.gov/docs/cgro/epo/vu/overview/whatare/process.html

[2] https://heasarc.gsfc.nasa.gov/docs/cgro/epo/vu/overview/whatare/process.html

each pulse describing a certain part of the GRB emission [3]. Studying the pulse properties of GRBs can help in understanding how the GRB mechanics works. This further emphasizes the importance of temporal analysis as studying these pulses can enhance our understanding of GRB physics. At the end of our analysis we will derive relations between different pulse properties and will evaluate them to derive useful results and further prove the analysis done by various authors.

[3] https://iopscience.iop.org/article/10.1086/377707/fulltext/57940.text.html#fg7

2. GAMMA-RAY BURSTS AND FERMI

2.1 Gamma-Ray Bursts Properties

GRBs were first discovered accidentally in the 1960's by the US military satellites and have opened a new door in high energy astrophysics since then. Gamma-Ray Bursts are extremely bright explosions which are hundred times brighter than a typical supernova explosion and are a million trillion times brighter than the Sun making them the brightest object in the observable universe [1]. A Gamma-Ray Burst emission can be divided into two main phases, the prompt emission and the afterglow. The prompt emission phase is that stage of the burst when Gamma rays are emitted and it lasts for a very short amount of time, a few seconds to minutes but the afterglow phase which can last from days to months includes the emission of x-rays, radio-waves and visible light. Based on the burst duration GRBs can be divided into two main categories, long and short GRBs. T90 duration is the duration criteria which is commonly used and shows the time interval in which 5% to 95% of the total fluence is observed during the prompt emission phase. Long GRBs have a T90 duration of greater than 2 seconds ($T90 > 2s$). Short GRBs on the other hand have a T90 duration of less than or equal to 2 seconds (T90$\leq$2s) [2].
Apart from the difference in T90 durations, different sources are attributed to the two categories. Long GRBs are believed to originate from stellar explosions or supernova and short from mergers of two compact objects in a binary system. The binary system can comprise of two neutron stars, or a black hole and a neutron star [2]. The merger of two black holes as a source of a short GRB has recently been detected by the Fermi Gamma-Ray Space Telescope [4].
The prompt emission phase is very short-lived (a few seconds to minutes),

[1] `https://imagine.gsfc.nasa.gov/science/objects/bursts1.html`

variable and complex, and is different for every GRB. This high variability makes generalizations about GRBs very hard through the analysis of the prompt emissions alone. On the other hand afterglow phase is longer with fairly smooth behavior [5]. Two processes essentially explain GRB mechanics: relativistic internal shocks and relativistic external shocks [6]. Internal shocks are described as the internal collisions of the GRB ejecta. External shocks are explained as the deceleration of the GRB ejecta due to the external medium. The amount of energy released in a GRB is typically observed in keV (Kilo-electron Volt) to MeV (Mega-electron Volt) energy range, even reaching up to TeV (Tera-electron Volt) in case of the highest energy GRBs. The first ever GRB in the TeV range was detected in 2018. The GRBs reaching TeV energy range include GRB 180720B, GRB 190114C (the GRB under study) and GRB 190829A [2]. More GRBs reaching this much energy are expected in the future. As only 3 TeV energy GRBs have been detected so far thus that raises our interest in understanding these GRBs and exploring the fact that whether these are any different from other GRBs or not becomes more important.
Looking at GRB distances these events occur at very large distances from earth and can occur at random locations. The typical distance of GRBs is 8 to 10 billion light-years with the closest GRB 030329 at a distance of 2.6 billion light-years [3].

2.2 The Fermi Detector

Space-based GRB detectors like Fermi (Fermi Gamma-Ray Space Telescope), Swift (Neil Gehrels Swift Observatory), CGRO (Compton Gamma-Ray Observatory) have been collecting Gamma-Ray Burst data for years among which Fermi is the latest one launched by NASA in 2008. Fermi consists of two main detectors, GBM (Gamma-Ray Burst monitor) and LAT (Large area telescope) with a combined energy range of 10 keV to 300 GeV which is a wider energy range compared to other space based grb detectors [4]. For higher energy ranges the two ground-based telescopes MAGIC (Major Atmospheric

[2] https://fermi.gsfc.nasa.gov/science/mtgs/symposia/2020/program/189/

[3] https://www.nrao.edu/pr/2003/grb030329/

[4] https://fermi.gsfc.nasa.gov/ssc/data/analysis/documentation/Cicerone/Cicerone_Introduction/GBM_overview.html

Gamma Imaging Cherenkov Telescope) come into action covering a broad energy range from 3GeV to 100 TeV [5]. GBM is expected to detect 200 GRBs every year complimenting LAT which is the primary instrument of the Fermi telescope [6]. For our analysis we will be using data from the GBM detector which further consists of 2 bismuth germanate (BGO) detectors and 12 sodium iodide (NaI) detectors. We will be using GBM data of the 4 NAI detectors (n3, n4, n7, and n8) based on the criteria of the strongest recorded emission. Each NAI detector is 12.7 cm in diameter by 1.27 cm thick. GBM provides low energy spectral and temporal measurements of GRBs within the LAT field of view (FOV) which is 20 percent of the sky. GBM also helps LAT in localizing and detecting GRBs by providing coarse GRB information on ground [7]. GBM together with LAT makes Fermi a very vital tool for Gamma-Ray Burst studies.

[5] https://www.mpp.mpg.de/en/research/astroparticle-physics-and-cosmology/magic-and-cta-Gamma-Ray-telescopes/magic/

[6] https://www.nasa.gov/content/goddard/fermi-spacecraft-and-instruments

[7] https://www.nasa.gov/content/goddard/fermi-spacecraft-and-instruments

3. PULSE PROPERTIES AND MODELS

3.1 Gamma-Ray Burst Pulse Characteristics

In this chapter we will discuss various pulse characteristics and models which will improve our understanding of GRB pulses and will help us in the performing temporal analysis on the GRB under study. Gamma-Ray Burst pulse structures are variable and every GRB is unique in its time profile [7]. That makes the study of Gamma-Ray Burst temporal evolution very interesting yet tricky. In our analysis of the Gamma-Ray Burst 190114C we will be working with light curves. In a light curve time is displayed on the x-axis and intensity which is energy per unit area per unit time or flux which is photons per unit area per unit time or simply counts which are photons/time can be displayed on the y-axis. The smallest unit in a Gamma-Ray Burst light curve is a pulse which we will study in depth.
The amplitude of a pulse is the peak of a pulse reached at the peak-time. The amplitude can be the maximum flux or intensity depending on what parameter we are using in our pulse model. Studying the properties of pulses within a light curve helps in uncovering vital information about a Gamma-Ray Burst. Some GRBs have very narrow overlapping pulses while some have wider pulses with simpler structure and some GRBs exhibit both of these behaviors as show in the figure below by [8].

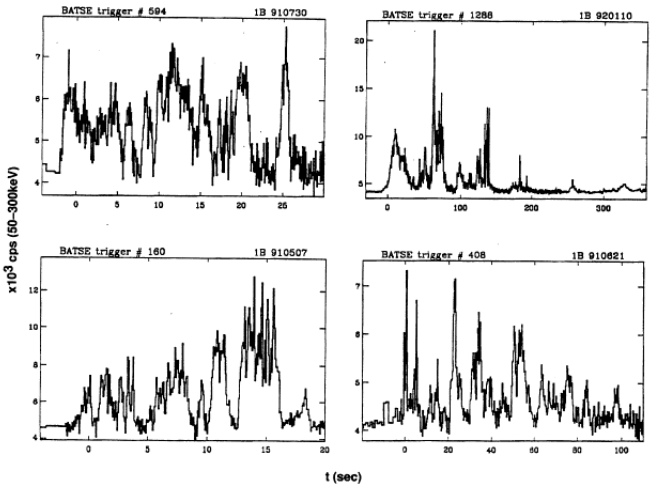

Figure 3.1: Overlapping, narrow pulses in some GRBs

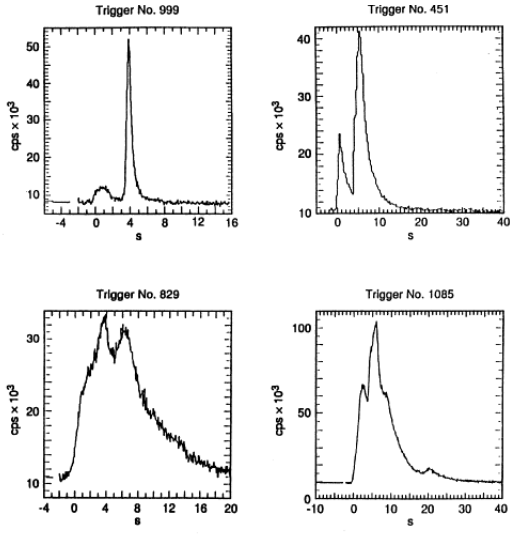

Figure 3.2: Simple pulse structures of some GRBs.

3.1.1 Full width at half maximum

The full width at half maximum is the width of a pulse at half the length to its peak [1]. Rise and decay time scales of a GRB pulse are generally related to the FWHM. This can be understood by the given image: [2].

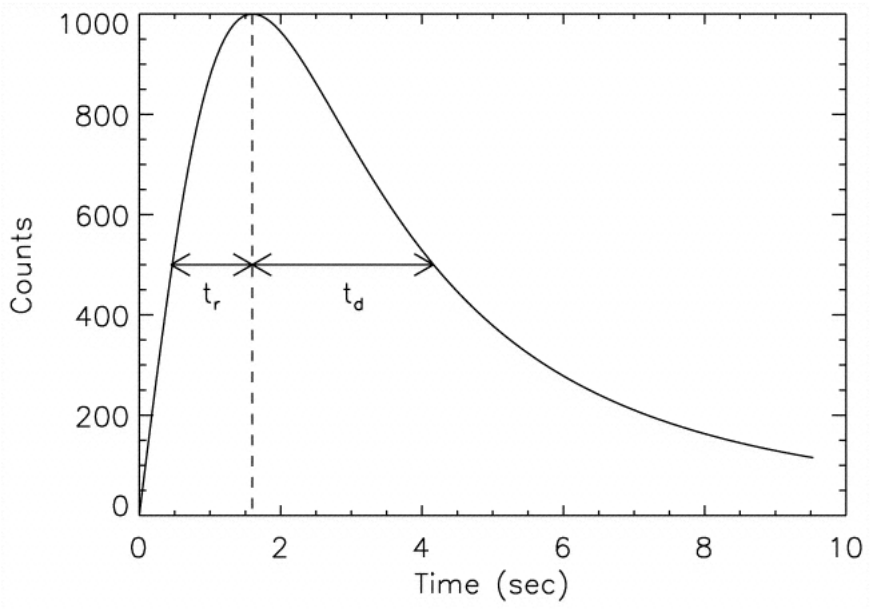

Figure 3.3: FWHM, with t-rise and t-fall.

Here we can see that at the FWHM we have time of rise till the peak time and after that we have the fall timescale. According to [9] the FWHM, rise time, fall/decay time and area of a pulse are directly related or have a positive correlation with each other while pulse amplitude and FWHM have a negative correlation or are inversely related with each other.

[1] https://www.noao.edu/image_gallery/text/fwhm.html

[2] https://iopscience.iop.org/article/10.1086/377707/fulltext/57940.text.html#fg7

3.1.2 Fast rise and exponential decay (FRED) pulses

Pulses which have a fast rise and decay slowly with a long tail are called FRED pulses. According to [10] FRED pulses are seen in long GRBs while the opposite behavior exponential rise and fast decay (ERFD) is seen in short GRBs. The symmetry of a pulse depends on its rise time to decay time ratio and in case of symmetric pulses the ratio is 1 but when we have a FRED or ERFD behavior in a pulse then the ratio of rise and fall time becomes less or greater than 1 giving us an asymmetric pulse.

3.1.3 Spectral lag

Spectral lag is a property observed in both long and short GRBs. Soft lag which means soft/low energy photons coming later than high energy/hard photons is observed in long GRBs as described by [1]. Hard-lag on the other hand is basically high energy photons lagging behind the soft photons and is observed in short GRBs as given in [11].

3.2 Temporal Models

Gamma-Ray Burst temporal models are useful approximations to explain their time evolution and the behavior of their pulses. Some of the temporal models that have been used by various researchers for temporal analysis are as follow:

3.2.1 Norris(2005)

This model is a widely used formula to study the pulse properties and temporal evolution of Gamma-Ray Bursts pulses, developed by [1]. The pulse model is as follow:

$$I(t) \quad = \quad A\lambda \exp\left(-\frac{\tau_1}{t-ts}\right) \exp\left(-\frac{t-ts}{\tau_2}\right) \quad \text{where } t > 0 \qquad (3.1)$$

Here ts is the pulse start time while τ_1 is the rise duration and τ_2 is the decay/fall duration of the pulse . A is the amplitude of the pulse which is actually the peak that a pulse reaches to as shown in figure 3.7a and $\lambda = exp(2\mu)$ where $\mu = (\tau_1/\tau_2)^{1/2}$. Here I(t) has units of amplitude. The two exponential terms indicate rising and decaying behavior of a pulse where $e^{-\frac{\tau_1}{t}}$ has a stronger effect on the rise and $e^{-\frac{t}{\tau_2}}$ has a stronger effect on the pulse decay. The two key factors of the model are τ_1 and τ_2 which decide the behavior of the pulse and from which pulse width w, asymmetry k and peak-time t_{pk} are derived. The peak intensity or amplitude can be calculated by taking the derivative of I(t), which becomes zero at the highest point giving us the peak time t_{peak}:

$$\frac{\mathrm{d}}{\mathrm{d}t}I(t) = \frac{\mathrm{d}}{\mathrm{d}t}\left[A\lambda \exp\left(-\frac{\tau_1}{t}\right)\exp\left(-\frac{t}{\tau_2}\right)\right] \tag{3.2}$$

$$0 = A\lambda\left[\frac{\mathrm{d}}{\mathrm{d}t}\exp\left(-\frac{\tau_1}{t}\right)\exp\left(-\frac{t}{\tau_2}\right)\right] \tag{3.3}$$

$$0 = \frac{\mathrm{d}}{\mathrm{d}t}\exp\left(-\frac{\tau_1}{t}\right)\exp\left(-\frac{t}{\tau_2}\right) \tag{3.4}$$

$$0 = \left(\frac{\tau_1}{t^2} - \frac{1}{\tau_2}\right)\exp\left(-\frac{\tau_1}{t}\right)\exp\left(-\frac{t}{\tau_2}\right) \tag{3.5}$$

$$0 = \frac{\tau_1}{t^2} - \frac{1}{\tau_2} \tag{3.6}$$

$$t = \sqrt{\tau_1\tau_2} \tag{3.7}$$

$$t_{\text{peak}} = \sqrt{\tau_1\tau_2} \tag{3.8}$$

The model described above has been used by many researchers including, [12], [13], [14], [15], [16] etc. Except for, [15] all the above studies include the λ value. In [15], λ has been removed and a parameter "B" has been added instead. Parameter B is the background radiation coming from sources other then the Gamma-Ray Burst under study. The formula used by [15] is given as following:

$$I(t) = A[\exp\left(-\frac{\tau_1}{t-t_s}\right)\exp\left(-\frac{t-t_s}{\tau_2}\right) + B] \qquad \text{when } t > t_s \tag{3.9}$$

$$= 0 \qquad \text{when } t < ts \tag{3.10}$$

In order to understand the Norris-2005 model we need to see how each variable effects the other. In the graphs given below we have varied τ_1, τ_2, amplitude and have removed λ in some plots to understand how these factors work. We have also studied the two exponential terms $\exp\left(-\frac{\tau_1}{t}\right)$ and

$\exp\left(-\frac{t}{\tau_2}\right)$ to see how these terms control the above model. In figure 3.4a and figure 3.4b we observe how the exponential terms in the model behave when τ_1 and τ_2 are varied and in figure 3.4c we explore λ.

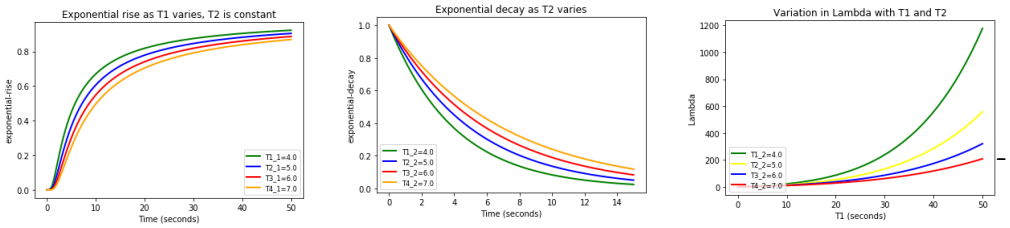

(a) (b) (c)

Figure 3.4: Observing relationships between $\exp\left(-\frac{\tau_1}{t}\right)$, τ_1, $\exp\left(-\frac{t}{\tau_2}\right)$, τ_2 and λ.

In figure 3.4a we observe that as τ_1 increases, the rise is delayed and the amplitude decreases as well which is due to the fact that we have a negative exponential. In figure 3.4b we observe that as τ_2 increases, the decay is delayed again due to the fact that we have a negative exponential.

In figure 3.4c as τ_1 increases along x-axis λ increases indicating a direct relation whereas when τ_2 increases, λ decreases, indicating an indirect relation. This effect is evident from the mathematical form $\lambda = exp(2\mu)$ where $\mu = (\tau_1/\tau_2)^{1/2}$.

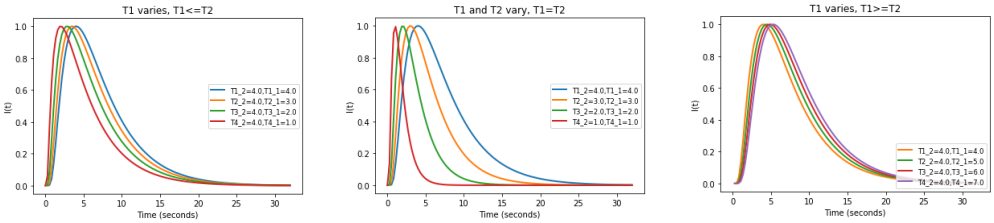

(a) (b) (c)

Figure 3.5: τ_1 is varied to observe the relationship between τ_1 and τ_2 .

In figure 3.5a, $\tau_1 \leq \tau_2$ which results in the rise duration of the pulse to be very small. The amplitude isn't affected. We also observe that the decay

duration are longer than the rise duration. In figure 3.5b, $\tau_1 = \tau_2$ but the decay duration is still longer. In figure 3.5c, $\tau_1 \geq \tau_2$ but the decay is still longer suggesting that the model under study is designed for asymmetric pulses. We also observe that t_{peak} varies as τ_1 varies but for larger values of τ_1 the variation is lesser. In figure 3.6a, $\tau_2 \leq \tau_1$ even then we see the decay duration is longer. The amplitude is unaffected. In figure 3.6b, $\tau_2 \geq \tau_1$ the decay duration is longer than in figure 3.6a . Just like in figure 3.5 for τ_1, t_{peak} also varies as τ_2 varies but that is again less for large values of τ_2.

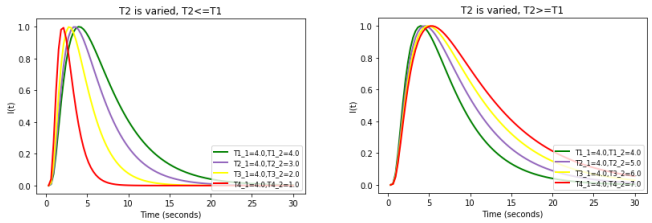

(a) (b)

Figure 3.6: τ_2 is varied to observe the relationship between τ_1 and τ_2.

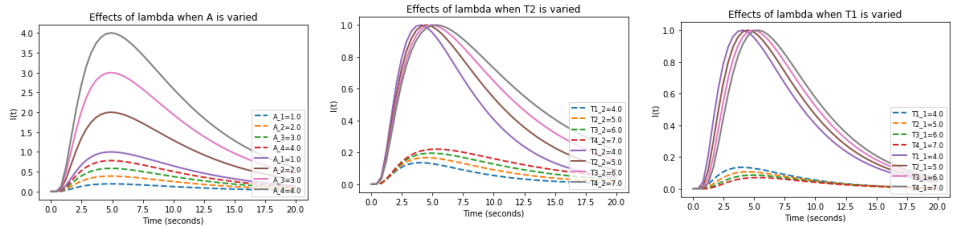

(a) (b) (c)

Figure 3.7: Effects of λ on τ_1, amplitude and τ_2 are observed. The dotted lines show plots without λ.

In figure 3.7a, when λ is removed the amplitude greatly decreases indicating that λ affects the amplitude. In figure 3.7b, when τ_2 is varied and λ is removed the peak time t_{peak} and amplitude both vary. While with λ when we vary τ_2 only t_{peak} varies. As τ_2 increases t_{peak} and amplitude increase. In figure 3.7c, when τ_1 is varied with λ we see that t_{peak} varies but when τ_1 is varied

without λ then amplitude varies as well. As τ_1 increases t_{peak} increases but amplitude decreases. These effects further confirm the conclusion made in figure 3.4a and in figure 3.4b .

3.2.2 Norris(1996)

This model developed by [7] is given as:

$$I(t) = A \exp\left[-(|t - t_{max}|/\sigma_r)^v\right] \quad t < t_{max} \tag{3.11}$$
$$= A \exp\left[-(|t - t_{max}|/\sigma_d)^v\right] \quad t > t_{max} \tag{3.12}$$

A is the amplitude or the peak of a pulse and has units of I(t) as the rest of the units are of time which get canceled. At $t = t_{max}$ we get the peak of the pulse. Here t_{max} is the peak timing of the pulse, σ_r is the rise and σ_d is the decay constant. This model has two conditions, when $t < t_{max}$ equation 3.11 will be used indicating the rise and when $t > t_{max}$ equation 3.12 will be used indicating the decay. The peakedness v shows the shape of the peak. This model has been used by [17] to study characteristic variability time scales and in the original paper to study the attributes of long and bright GRBs. We study the different parameters used in the model by varying each quantity to evaluate its effect. We vary σ_r, σ_d, amplitude, t_{max} and v to understand their role in the model. While one variable is varied the rest are kept constant.

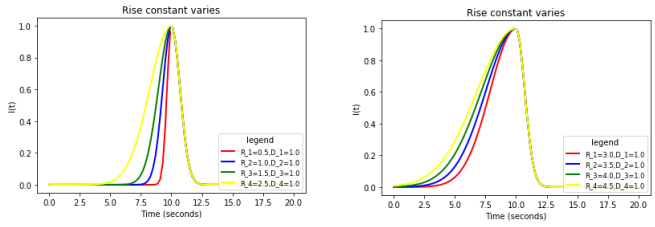

(a) (b)

Figure 3.8: σ_r is varied to understand how it affects the pulse evolution.

In figure 3.8 we observe that as σ_r which is the rise constant increases, the rise duration increases and the pulse also rises early. In figure 3.8b we see the same effect amplified as σ_r increases further. No affect is observed on decay and amplitude in both images. This shows that the σ_r affects the

rise duration only. In figure 3.9a and figure 3.9b as σ_d increases the decay duration increases with no affect on amplitude and rise duration. In figure 3.10a as amplitude is varied the peak value of the pulse varies as expected. In figure 3.10b when peakedness value v increases the pulse peak becomes flatter. In figure 3.10c as t_{max} increases the pulse peak time increases.

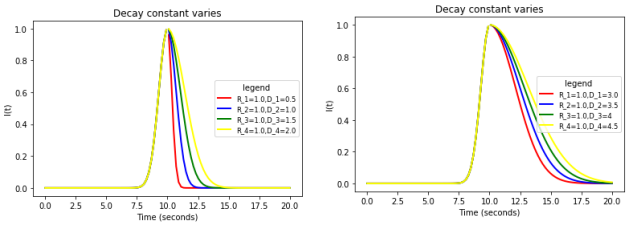

(a) $\sigma_d < \sigma_r$ (b) $\sigma_d > \sigma_r$

Figure 3.9: Effects of σ_d on decay duration amplitude and rise duration.

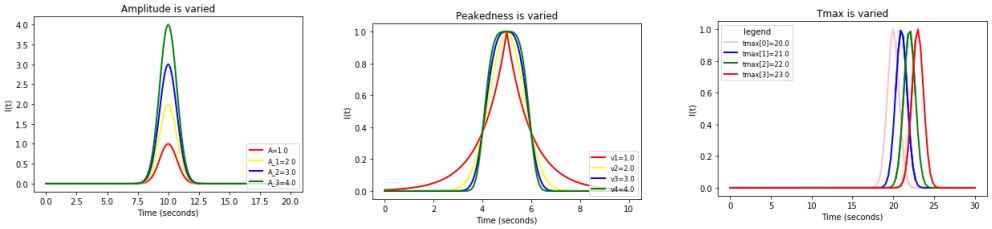

(a) (b) (c)

Figure 3.10: Amplitude A, Peakedness v and peak time of a pulse t_{max} are varied.

3.2.3 Log-normal model

This model developed by [18] is given as:

$$f(t) = \frac{A}{\sqrt{2\pi}t\sigma}\exp\left(-\frac{(logt-\mu)^2}{2\sigma^2}\right) \qquad t>0 \tag{3.13}$$

$$= 0 \qquad t \leq 0 \tag{3.14}$$

Here A is the amplitude, σ is the standard deviation of log(t) and μ is the mean of log(t).
In figures below we study σ, μ and amplitude to understand how the model is controlled by these factors. In figure 3.11a, as amplitude increases the pulse peak rises which was straightforward. We observe usual behavior of amplitude. In figure 3.11b, μ which is the mean of log(t) when increased, increases both amplitude and width of the pulses. The behavior of σ is not easy to understand as increasing it increases amplitude but decreases width.

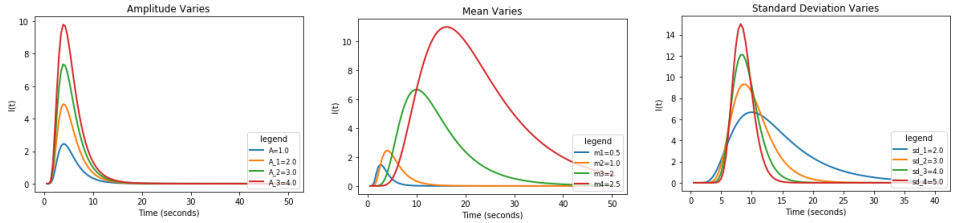

(a) (b) (c)

Figure 3.11: Amplitude A, standard deviation σ and mean μ are varied.

3.2.4 Flux Variability Model

This particular model has been used to study blazars and Gamma-Ray Bursts. The model as given in [19] is as follow:

$$F(t) = F_0 + \frac{b}{\exp\left(-\frac{(t-t_o)}{t_r}\right) + \exp\left(\frac{t-t_o}{t_f}\right)} \tag{3.15}$$

Here $F(t)$ is the flux, t_o is the actual peak time of symmetric pulses but gives an approximation of peak time for asymmetric pulses as well. t_r is rise and t_f is the fall time. In the figures below we study t_f, t_r, F_0 and b to understand the characteristics of the model. In figure 3.12, t_r is varied. As t_r increases the amplitude and rise durations increase also the pulse rises early when t_r is large. As t_r rises much greater than t_d we see negligible effect of variation in t_r on rise durations, amplitude and on the pulse rise time.
In figure 3.13, t_d is varied. As it increases the decay duration decreases, the decay occurs early along with decrease in amplitude. For higher values of t_d this effect becomes negligible. In figure 3.14 and in figure 3.15 we explore F_0 and b. Their behavior is easy to understand. In figure 3.14 F_0 effects the initial flux, increasing it increases the initial flux while in figure 3.15 increasing b increases the amplitude.

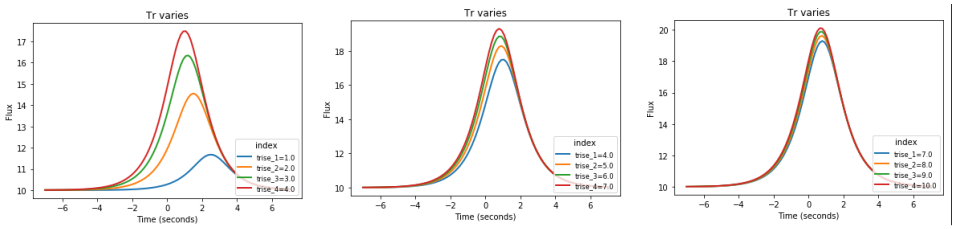

(a) $t_r \leq t_d$ (b) $t_r \geq t_d$ (c) $t_r > t_d$

Figure 3.12: t_r is varied which strongly affects the rise of the pulses.

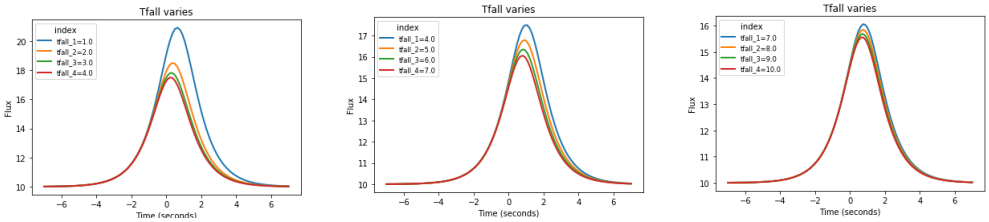

(a) $t_d \leq t_r$ (b) $t_d \geq t_r$ (c) $t_d > t_r$

Figure 3.13: t_d is varied which dominantly affects the decay of the pulses.

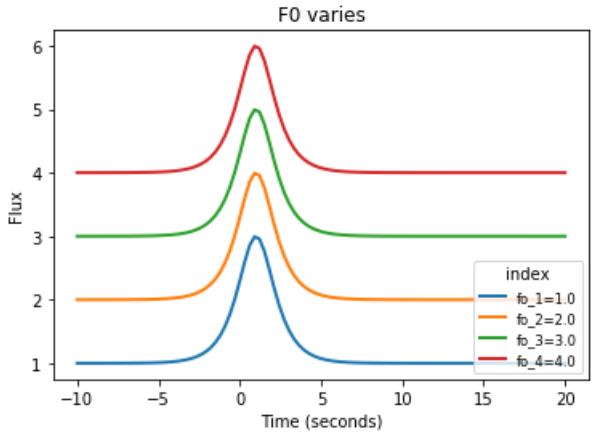

Figure 3.14: F_0 is varied.

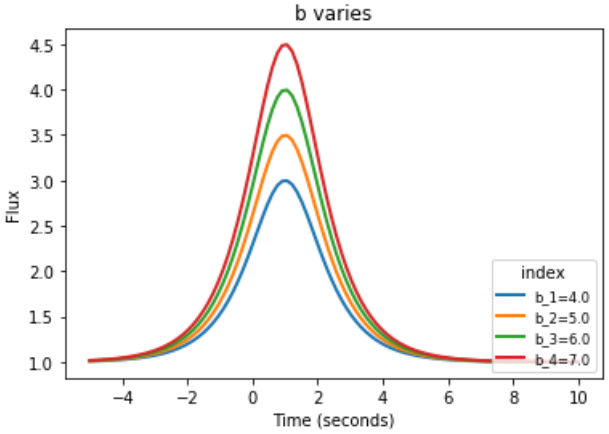

Figure 3.15: b is varied.

4. TEMPORAL ANALYSIS

4.1 Gamma-Ray Burst Data

In this chapter we will explain each step of our analysis in detail from data-selection to background and GRB signal fitting. Using the Norris-2005 model as described in the previous chapter we will explore the temporal profile of the GRB 190114C. The Fermi telescope consists of two main detectors, GBM (Gamma-Ray Burst monitor) and LAT (large area telescope) with a combined energy range of a few keV to 300 GeV [1]. For our analysis we have used data from the 4 NAI (sodium iodide) detectors part of the GBM(Gamma-Ray Burst monitor) detector within Fermi.
The approximate energy range of NAI is from a few KeV to 1 MeV [2]. The 4 NAI detectors n3, n4, n7 and n8 showed the strongest signal as shown in figure: 4.1 [3]. Here we can see the signal is the strongest with the highest peaks in n3, n4, n7 and n8 making them the right choice for our analysis. Looking at figure 4.3 it will become clear that in order to see the entire structure including the low intensity pulse at the end, NAI data is the right choice as in case of BGO data, the 2nd structure was somewhat lost.

[1] https://fermi.gsfc.nasa.gov/ssc/data/analysis/documentation/Cicerone/Cicerone_Introduction/GBM_overview.html

[2] https://fermi.gsfc.nasa.gov/science/instruments/gbm.html

[3] https://heasarc.gsfc.nasa.gov/FTP/fermi/data/gbm/triggers/2019/bn190114873/quicklook/glg_lc_all_bn190114873.gif

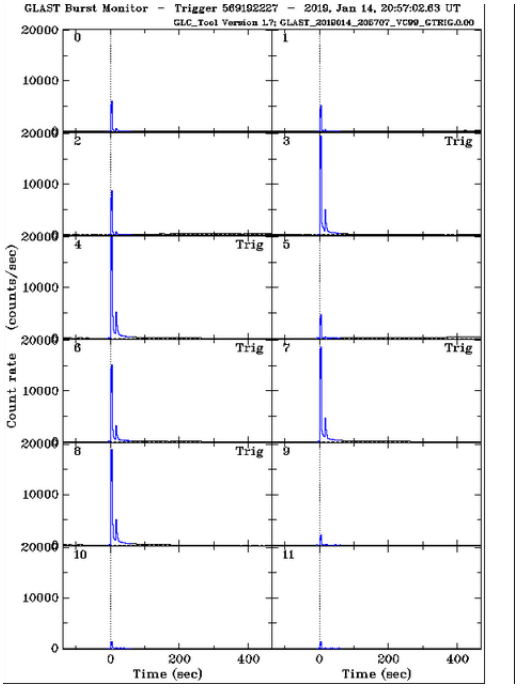

Figure 4.1: GRB signal in all NAI detectors

4.2 Background-fitting and Time Binning

We have performed fitting of the background signal of our GRB using the Rmfit software. First we made cuts before and after the T90 duration (117 seconds approx) of our GRB signal to specify the background as shown in figure:4.2. Afterwards we selected a 2 degree polynomial for fitting the selected background. The polynomial is predefined in the system we only need to select the degree. For time binning we selected the binning of 0.09 seconds as it gave the highest number of pulses with the the highest clarity making visual identification of pulses easier.

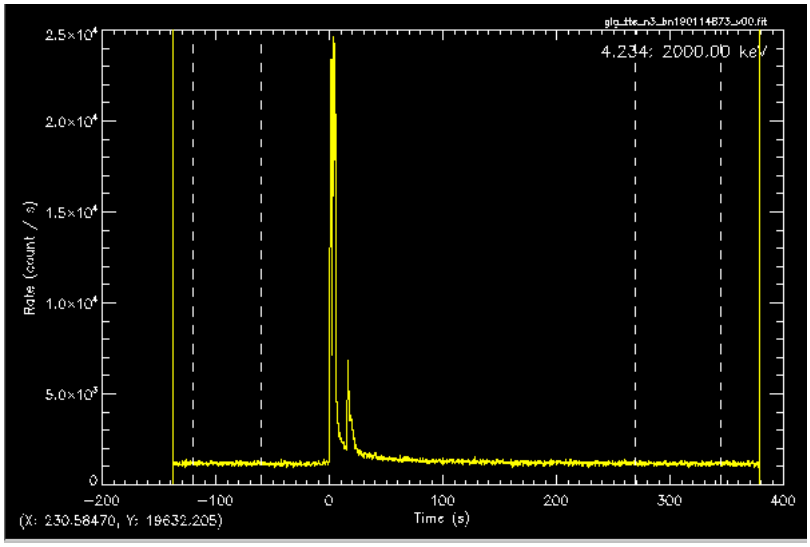

Figure 4.2: Background selection in Rmfit

4.3 Light-Curves

Once the background is fitted we developed light curves using python where we summed the data from the n3, n4, n7 and n8 detectors to construct counts vs time plots. For this particular plot we have used the enitre NAI range of 8-930 KeV as given in figure: 4.3. The light curve showed two major phases, the first one is the multi-peaked structure with very narrow, high amplitude pulses. The 2nd is the smaller structure with a much wider pulse and a very small amplitude. This indicates that in a GRB with time, pulse width will increase and amplitude will decrease.

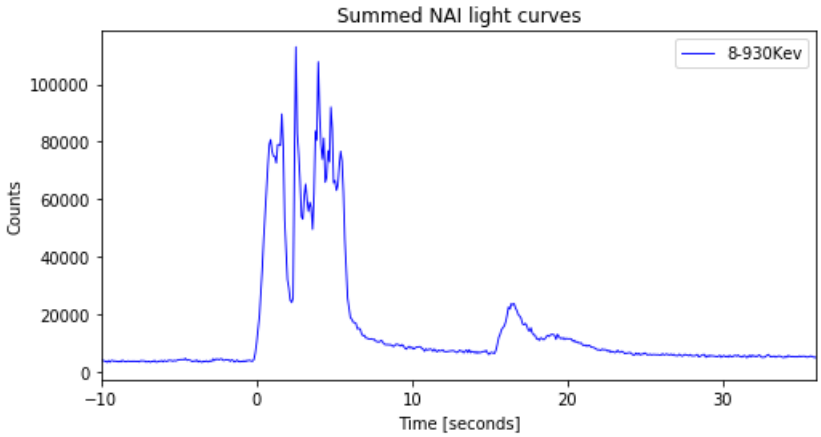

Figure 4.3: GRB 191014C light-curve

4.4 Curve-fitting with Norris-2005 and Pyroot

After background fitting we started the curve-fitting process in which we used the Norris-2005 model. The curve-fitting process is crucial as it uses a model to define ideal behavior of data, takes in initial guesses for the parameters (we entered 4 guess parameters) and and gives us pulse parameters for our given data like amplitude, rise, start time and decay duration in our case. The parameters depend on the choice of the model. These parameters are used to understand the behavior of our GRB with time which will be described in detail ahead. The Norris-2005 model has the functional form as explained in the previous chapter:

$$I(t) = A\lambda \exp\left(-\frac{\tau_1}{t-ts}\right) \exp\left(-\frac{t-ts}{\tau_2}\right) \quad \text{where } t > 0 \tag{4.1}$$

The width and asymmetry which are the two shape parameters of this model are given by:

$$w = \tau_2(1+4\mu)^{1/2} \tag{4.2}$$

$$k = (1+4\mu)^{1/2} \tag{4.3}$$

$$= \frac{\tau_2}{w} \tag{4.4}$$

We will calculate the above parameters for each pulse in our GRB signal with the help of the curve-fitting procedure.

4.4.1 Fitting results in different energy channels

Using similar energy channels as used by [18] we have carried out curve-fitting by choosing 5 energy channels to see the changes in the pulses. The fitting results for the energy channels "8-20 KeV", "20-40 KeV", 40-142 KeV", "142-524 KeV" and 524-930 KeV" are given below. We can see that as the energy level increases the number of pulses increase. The fitting results look appropriate visually. The resultant parameters are also given in the tables below. We found out pulse start time, rise duration, decay duration, ampltude, width and asymmetry using the Norris-2005 model. We observe in the fitted curves below that as the energy is raised the pulses become narrower indicating a decrease in width. From the energy channel 8-20 KeV to 20-40 KeV we observe an increase in amplitude. From 20-40 KeV to 40-142 KeV we see the amplitude increase is very high as the energy band is wider. In the energy band of 40-142 KeV to 142-524 KeV we see amplitude decrease and in the energy band 524-930 KeV the amplitude is the lowest of all the energy bands. This indicates that the number of photons detected per second by the Fermi GBM is the highest in the energy range showing the greatest number of photon counts which is 50,000 per second in the case of the energy band of 40-142 KeV. In the next chapter we will explain the results and the relationships between the parameters derived by the curve-fitting procedure in detail.

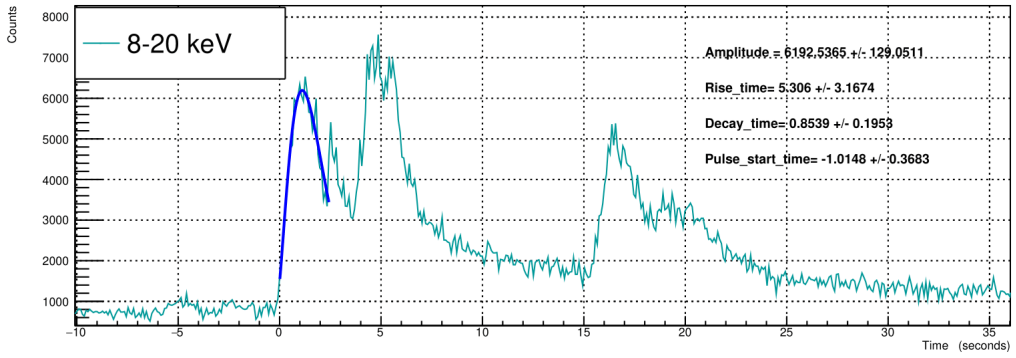

Figure 4.4: Pulse-1

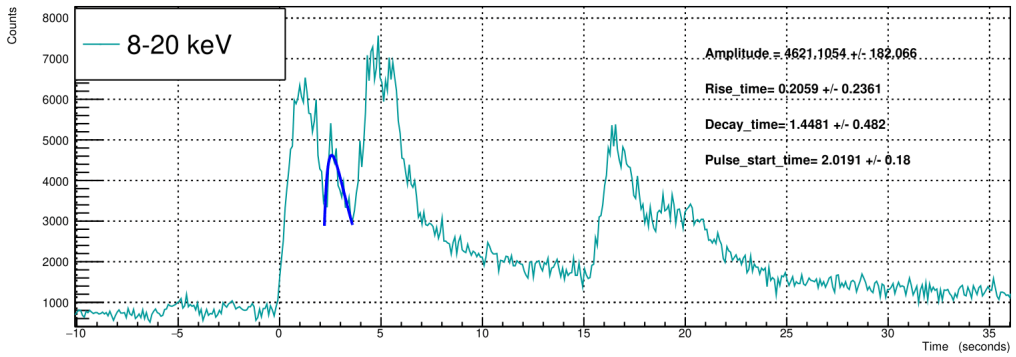

Figure 4.5: Pulse-2

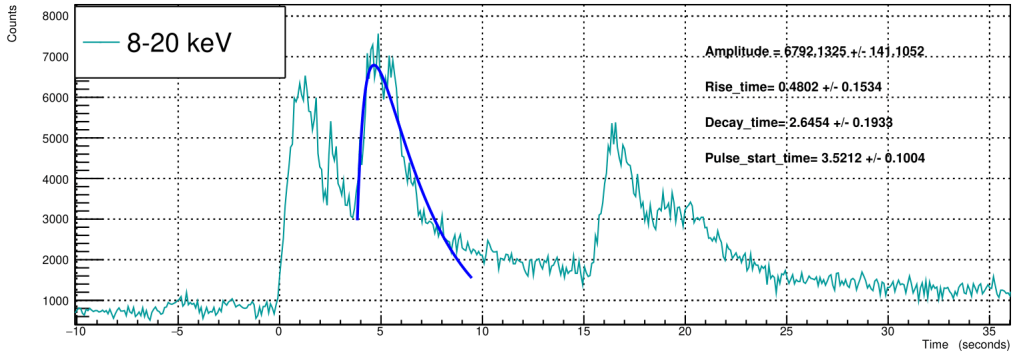

Figure 4.6: Pulse-3

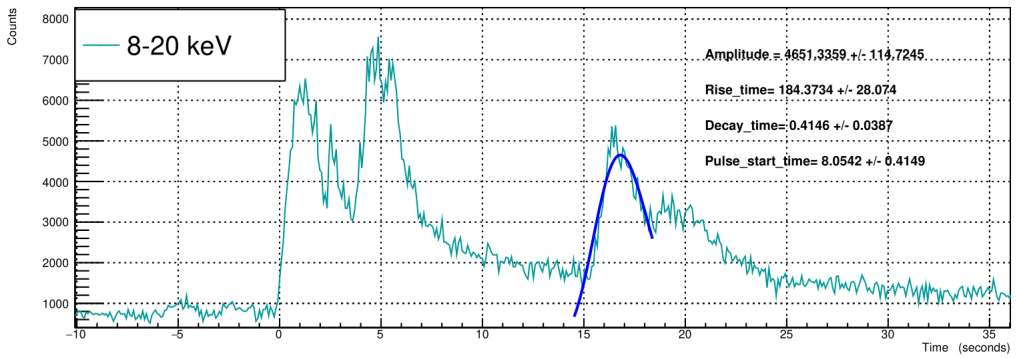

Figure 4.7: Pulse-4

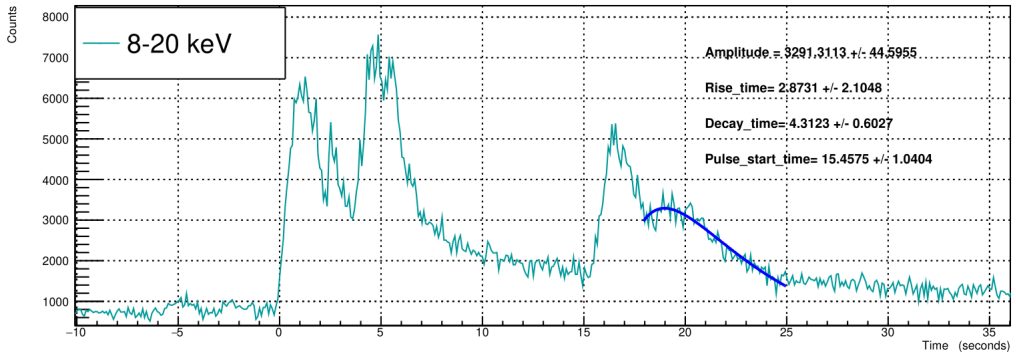

Figure 4.8: Pulse-5

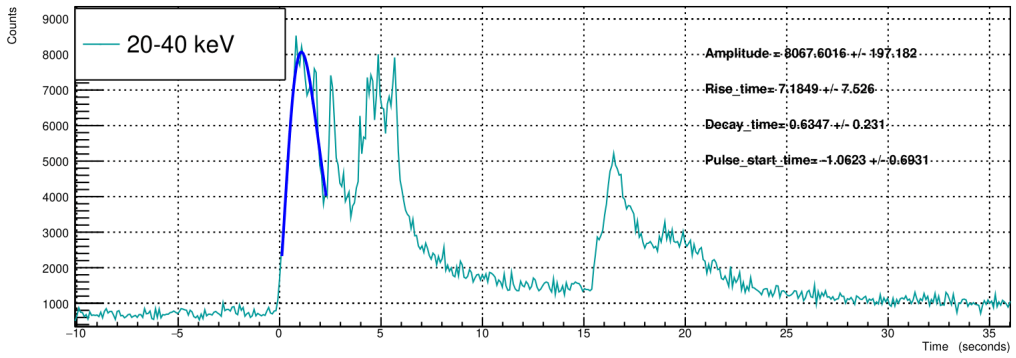

Figure 4.9: Pulse-1

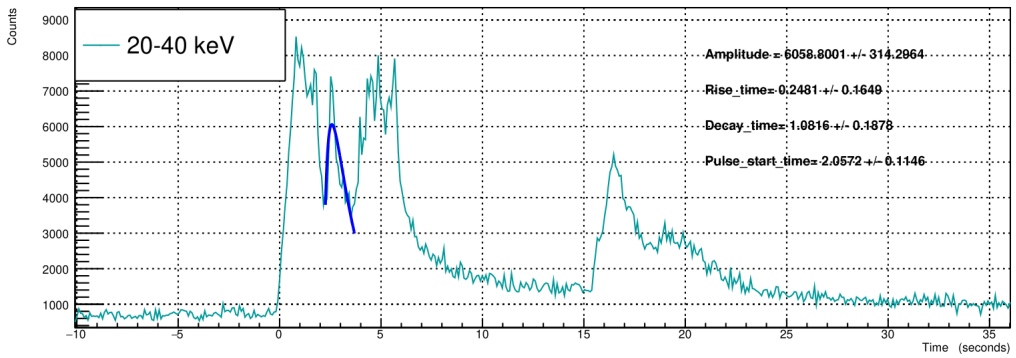

Figure 4.10: Pulse-2

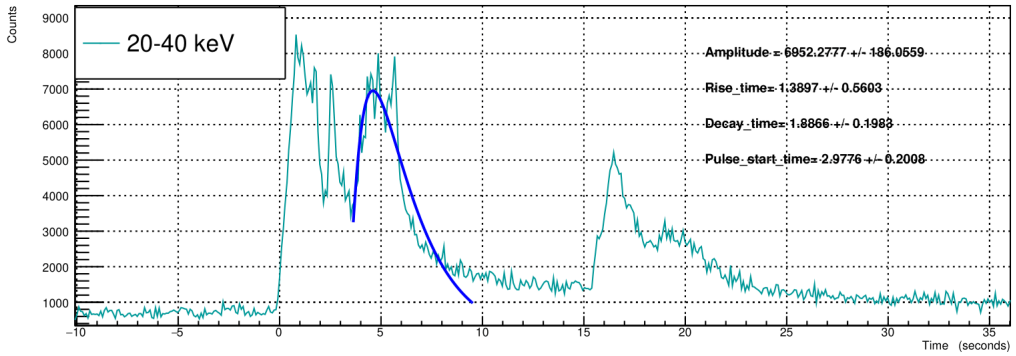

Figure 4.11: Pulse-3

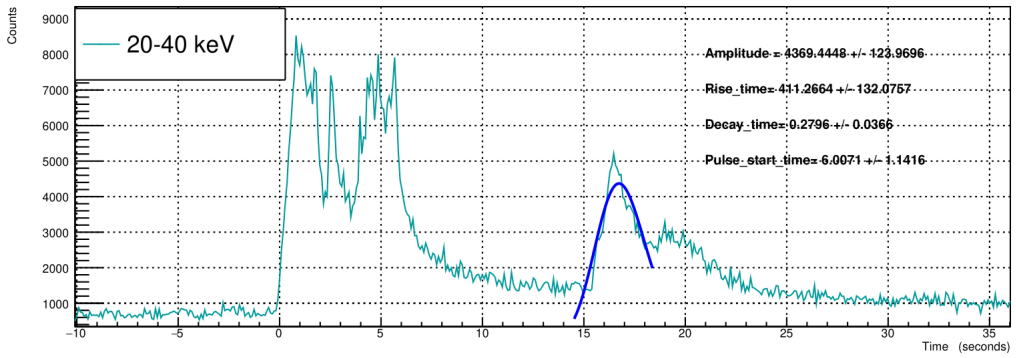

Figure 4.12: Pulse-4

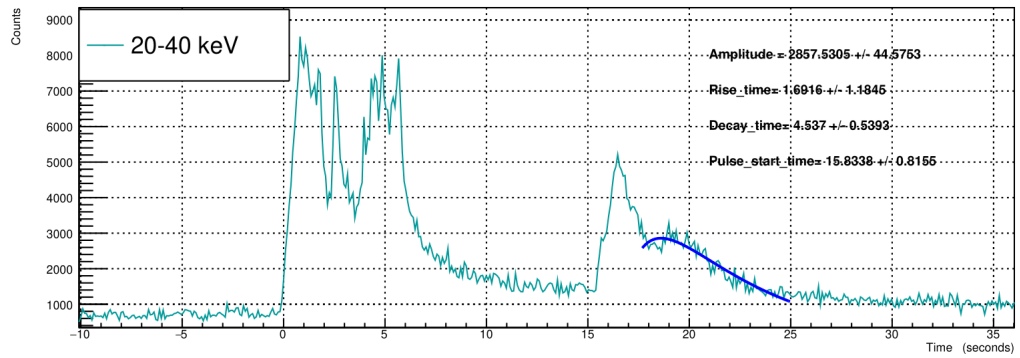

Figure 4.13: Pulse-5

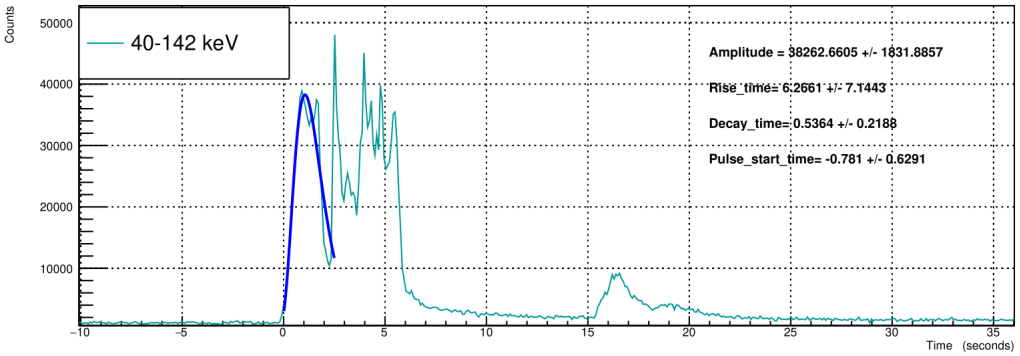

Figure 4.14: Pulse-1

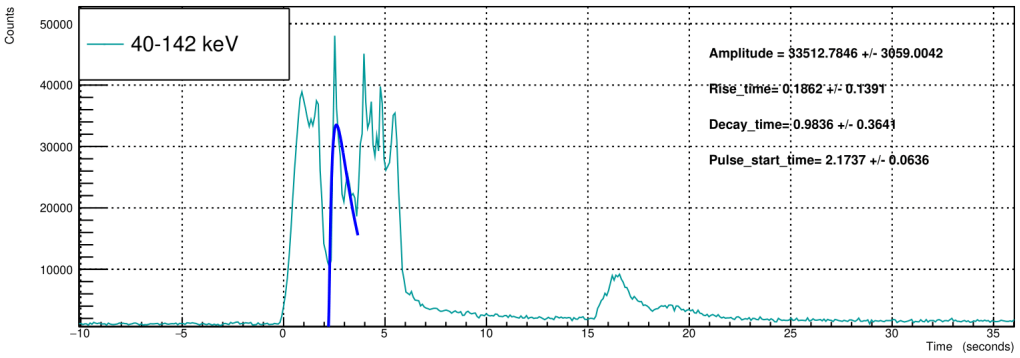

Figure 4.15: Pulse-2

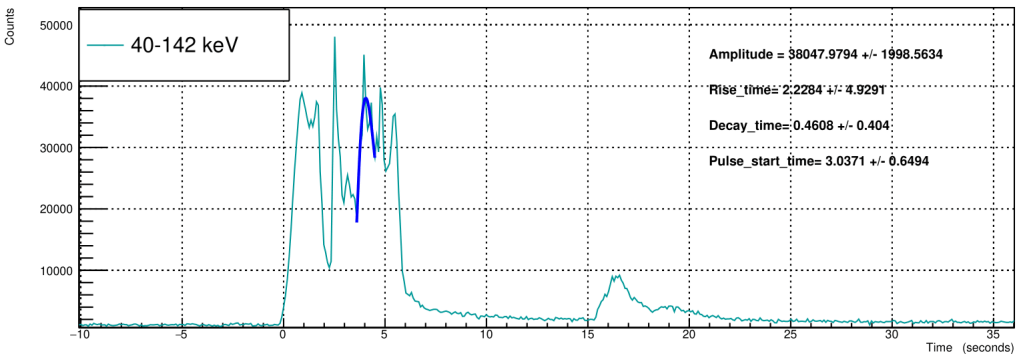

Figure 4.16: Pulse-3a

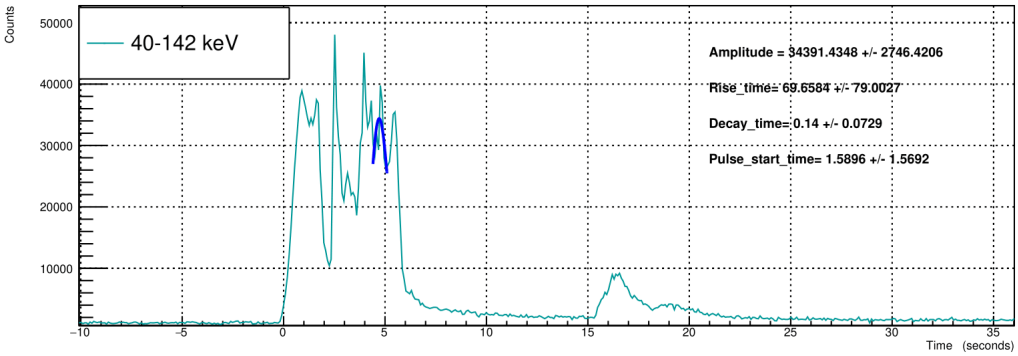

Figure 4.17: Pulse-3b

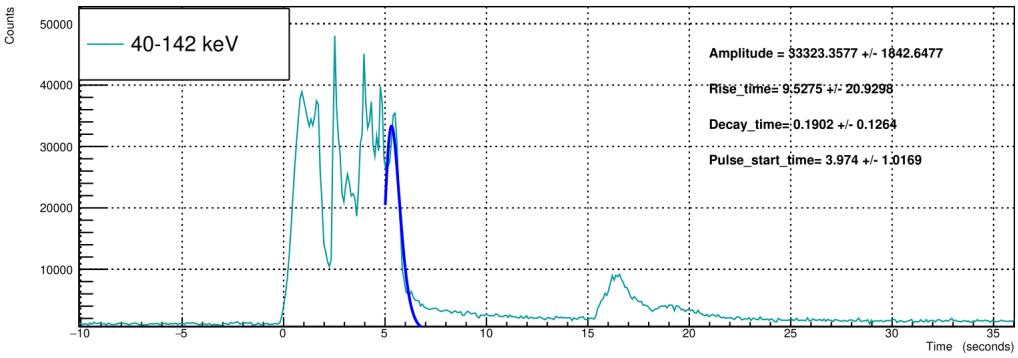

Figure 4.18: Pulse-3c

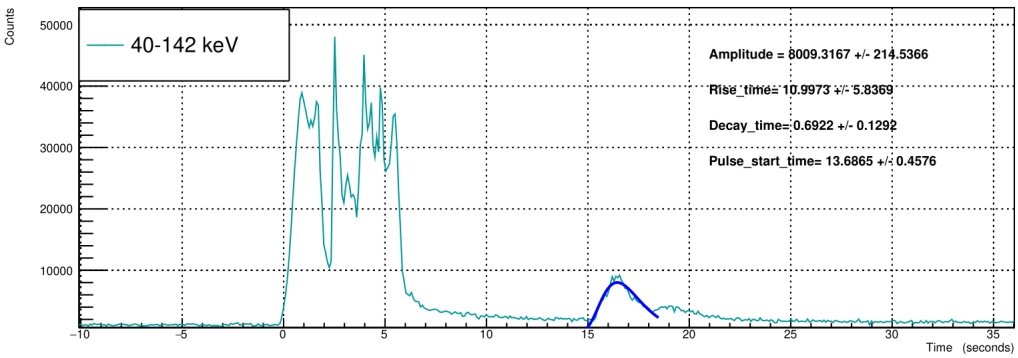

Figure 4.19: Pulse-4

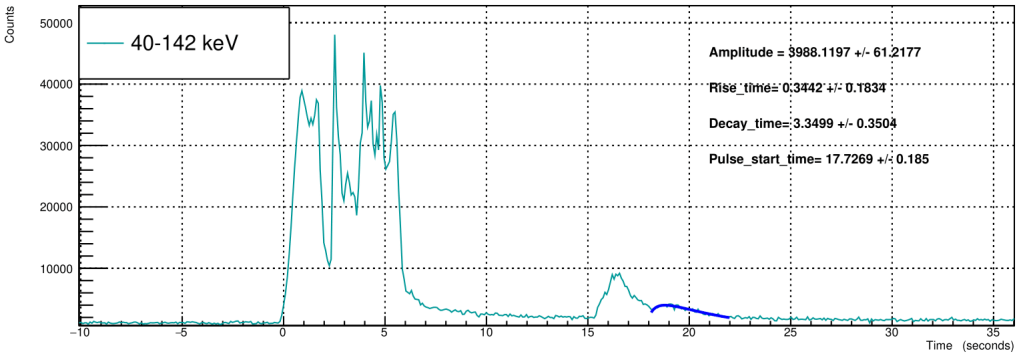

Figure 4.20: Pulse-5

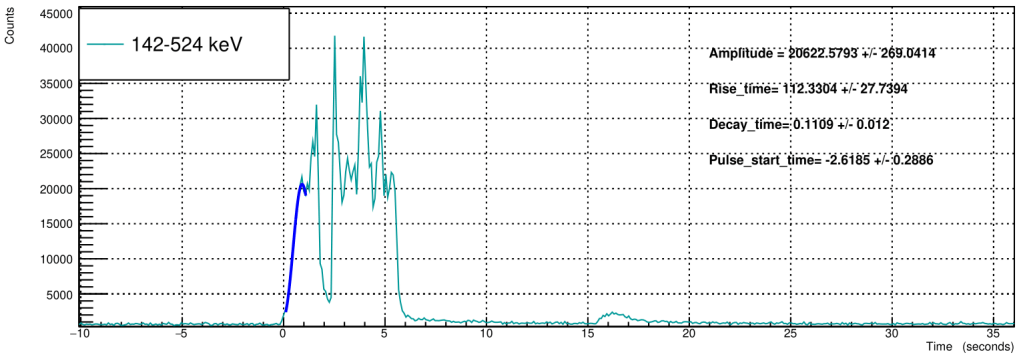

Figure 4.21: Pulse-1a

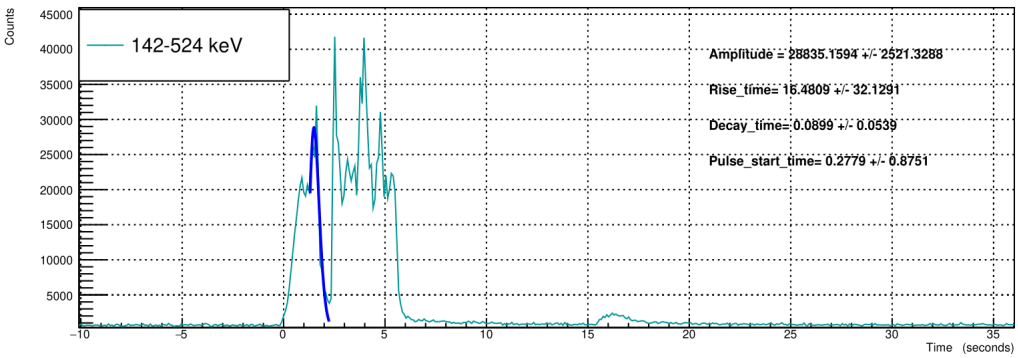

Figure 4.22: Pulse-1b

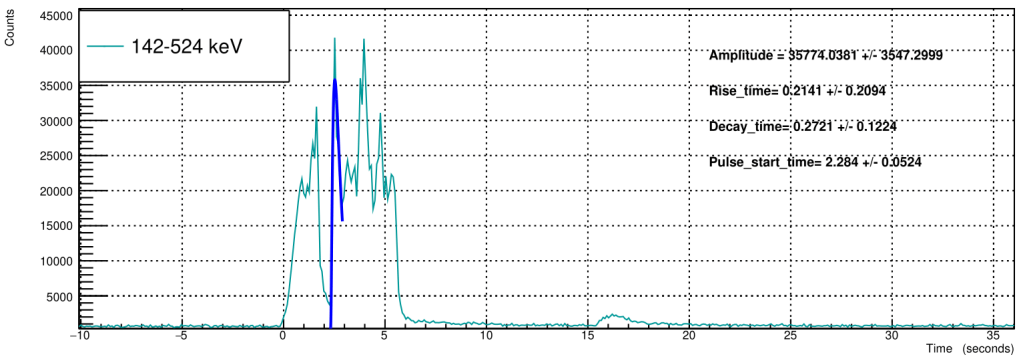

Figure 4.23: Pulse-2a

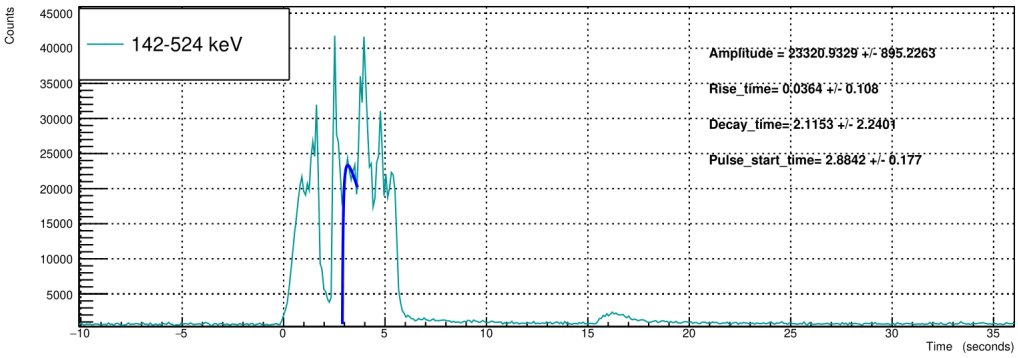

Figure 4.24: Pulse-2b

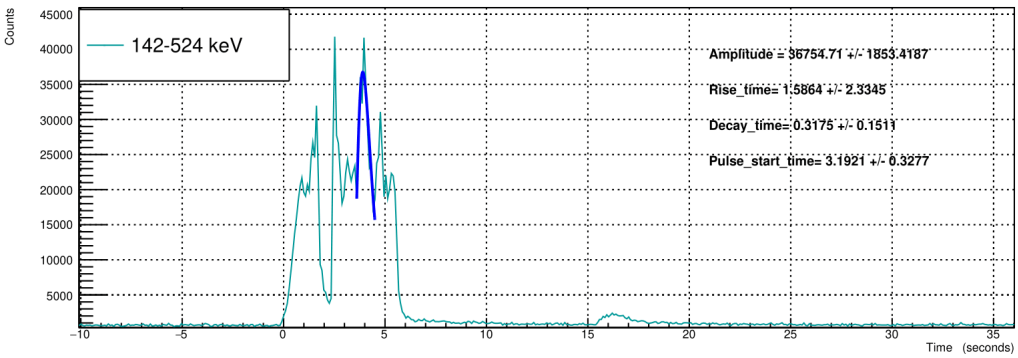

Figure 4.25: Pulse-3a

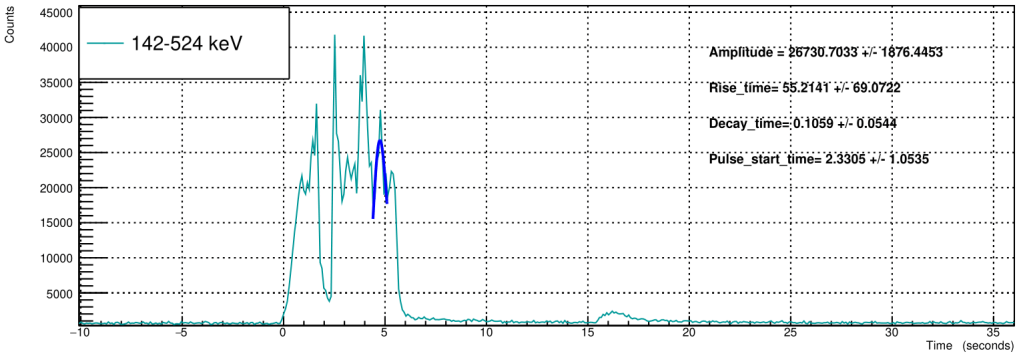

Figure 4.26: Pulse-3b

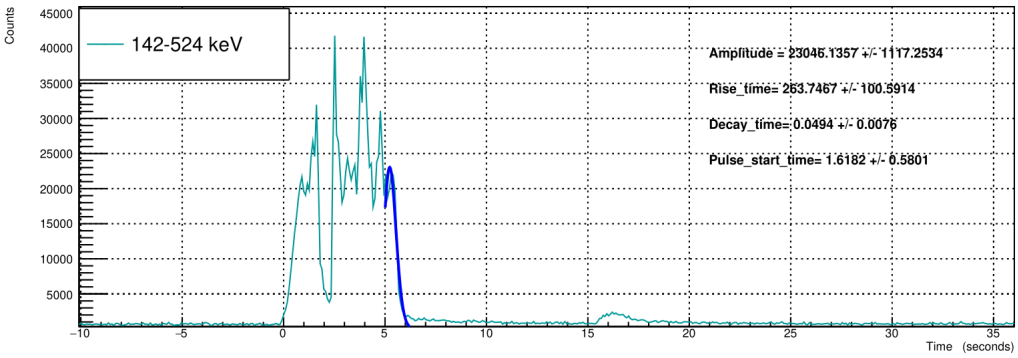

Figure 4.27: Pulse-3c

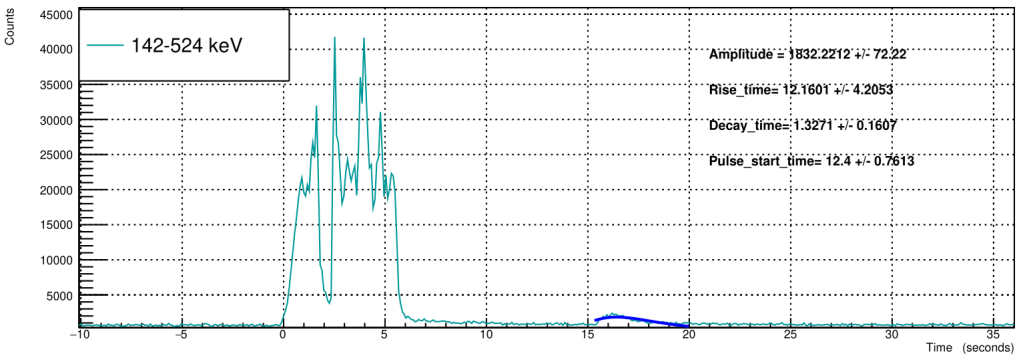

Figure 4.28: Pulse-4

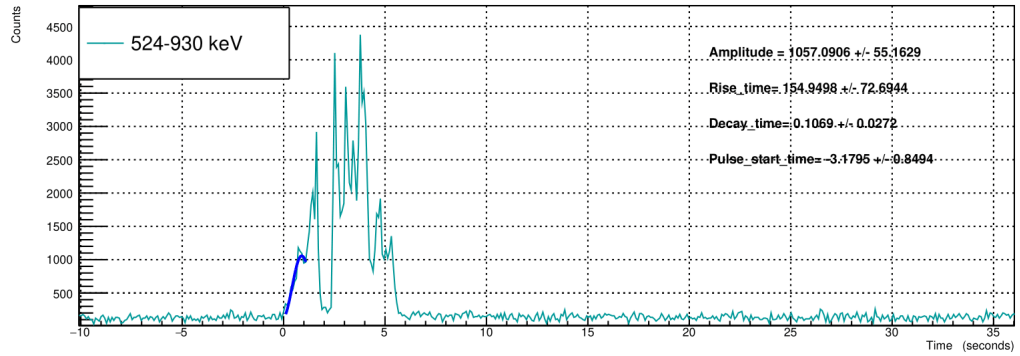

Figure 4.29: Pulse-1a

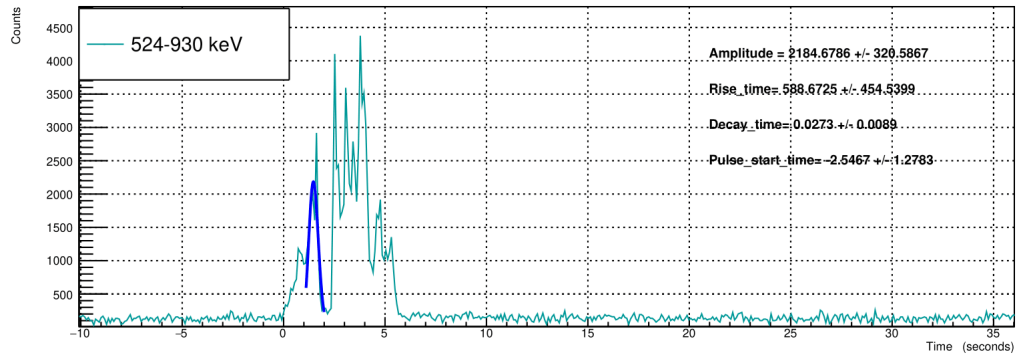

Figure 4.30: Pulse-1b

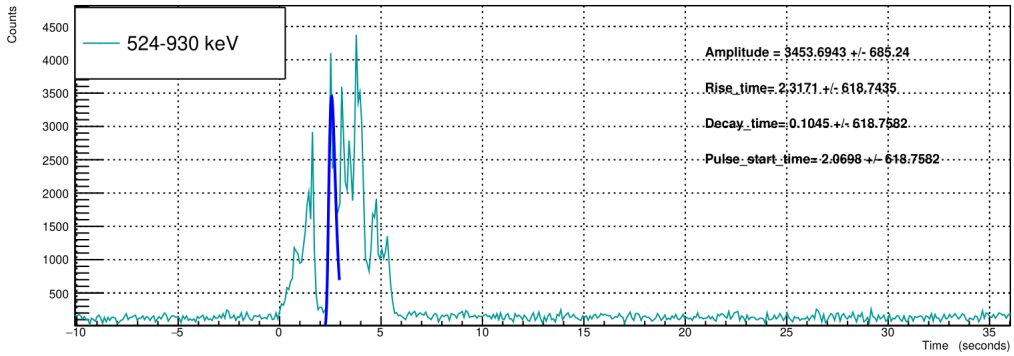

Figure 4.31: Pulse-2a

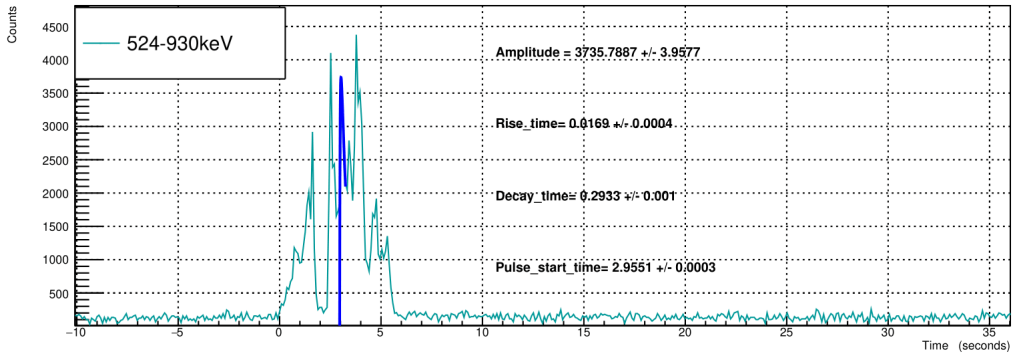

Figure 4.32: Pulse-2b

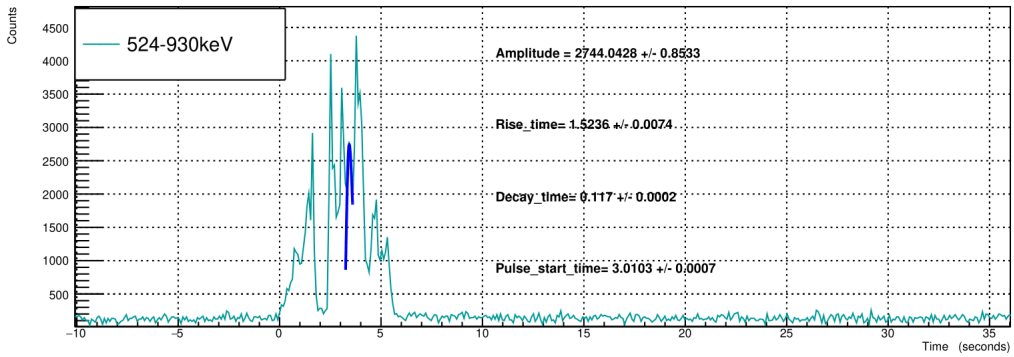

Figure 4.33: Pulse-2c

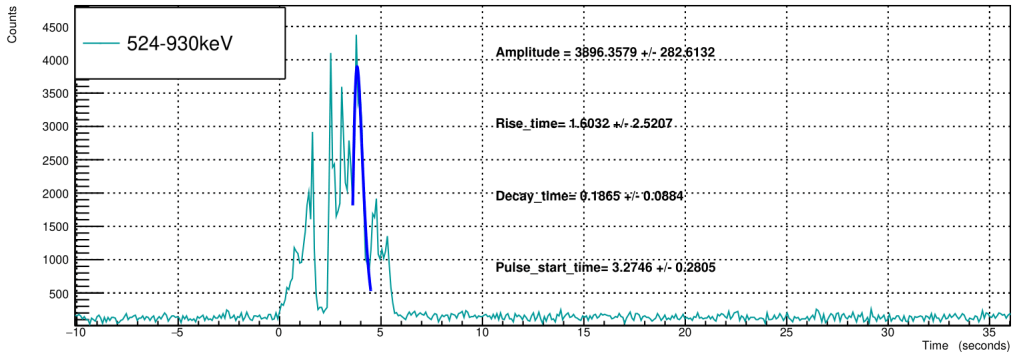

Figure 4.34: Pulse-2d

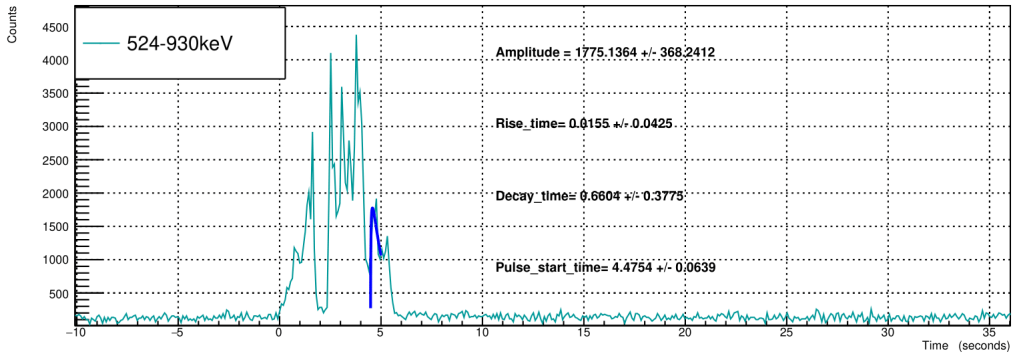

Figure 4.35: Pulse-3a

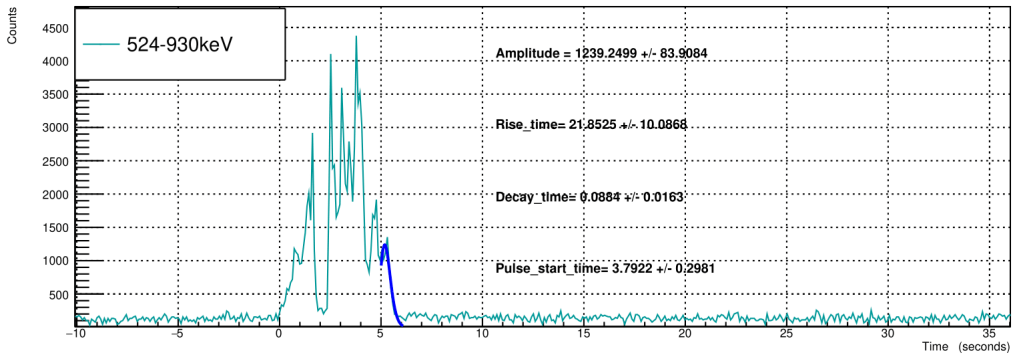

Figure 4.36: Pulse-3b

8-20kev	ts	T1	T2	amplitude	width	asymmetry	Chi-2	NDF	Edm	Ncalls
pulse-1	-1.0148 +/- 0.3683	5.3060 +/- 3.1674	0.8539 +/- 0.1953	6192.54 +/- 129.051	2.8282 +/- 0.8077	0.3019 +/- 0.2418	3.76514e+ 06	24	5.96515e-07	604
pulse-2	2.0191 +/- 0.1800	0.2059 +/- 0.2361	1.4481 +/- 0.4820	4621.11 +/- 182.066	2.2934 +/- 0.9396	0.6314 +/- 0.5130	2.13093e+ 06	12	7.82705e-07	1471
pulse-3	3.5212 +/- 0.1004	0.4801 +/- 0.1534	2.6454 +/- 0.1933	6792.13 +/- 141.105	4.3502 +/- 0.4129	0.6081 +/- 0.4681	1.6524e+0 7	59	7.41126e-07	981
pulse-4	8.0541 +/- 0.4149	184.37 +/- 28.074	0.4146 +/- 0.0386	4651.34 +/- 114.724	3.8304 +/- 0.4032	0.1082 +/- 0.0958	8.24122e+ 06	39	10031.7	1485
pulse-5	15.4575 +/- 1.04036	2.8731 +/- 2.1049	4.3129 +/- 0.6027	3291.31 +/- 44.5955	0.8562 +/- 1.7546	5.0360 +/- 0.3435	3.05441e+ 06	75	8.29343e-06	1486

Figure 4.37: Curve-fitting results for 8-20 KeV energy channel

20-40kev	ts	T1	T2	amplitude	width	asymmetry	Chi-2	NDF	Edm	Ncalls
pulse-1	-1.0623 +/- 0.6931	7.1849 +/- 7.5259	0.6346 +/- 0.2310	8067.6 +/- 197.182	2.4132 +/- 1.1278	0.2629 +/- 0.2048	6.65325e+ 06	20	5.20037e-07	811
pulse-2	2.0572 +/- 0.1146	0.2481 +/- 0.1649	1.0816 +/- 0.1878	6058.8 +/- 314.296	1.8468 +/- 0.4092	0.5856 +/- 0.4589	7.42401e+ 06	13	151481	1481
pulse-3	2.9776 +/- 0.2008	1.3897 +/- 0.5603	1.8866 +/- 0.1983	6952.28 +/- 186.056	3.9722 +/- 0.5511	0.4749 +/- 0.3598	3.1827e+0 7	63	2.83471e-07	1085
pulse-4	6.0071 +/- 1.1416	411.266 +/- 132.076	0.2796 +/- 0.0366	4369.44 +/- 123.97	3.4740 +/- 0.5682	0.0805 +/- 0.0643	8.70137e+ 06	39	1100.2	1482
pulse-5	15.8338 +/- 0.8155	1.6916 +/- 1.1845	4.5370 +/- 0.5393	2857.53 +/- 44.5753	0.5187 +/- 1.4195	8.7468 +/- 0.3799	2.92236e+ 06	77	1.90718e-07	1276

Figure 4.38: Curve-fitting results for 20-40 KeV energy channel

40-142kev	ts	T1	T2	amplitude	width	asymmetry	Chi-2	NDF	Edm	Ncalls
pulse-1	-0.7809 +/- 0.6291	6.2661 +/- 7.1443	0.5364 +/- 0.2188	38262.7 +/- 1831.89	2.0544 +/- 1.0685	0.2610 +/- 0.2047	7.05309e+08	24	1.36418e-06	597
pulse-2	2.1737 +/- 0.0636	0.1862 +/- 0.1391	0.9836 +/- 0.3641	33512.8 +/- 3059	1.6283 +/- 0.6784	0.6040 +/- 0.5366	5.28417e+08	12	4.37634e-07	1186
pulse-3a	3.0371 +/- 0.6494	2.2284 +/- 4.9291	0.4608 +/- 0.4040	38048 +/- 1998.56	1.4421 +/- 1.5632	0.3195 +/- 0.2584	1.11247e+08	7	7.10859e-10	659
pulse-3b	1.5896 +/- 1.5692	69.6584 +/- 79.0027	0.1399 +/- 0.0729	34391.4 +/- 2746.42	1.3298 +/- 0.8394	0.1052 +/- 0.0868	9.96488e+07	4	105404	1490
pulse-3c	3.9739 +/- 1.0168	9.52752 +/- 20.9298	0.1901 +/- 0.1264	33323.4 +/- 1842.65	1.0295 +/- 0.9154	0.1847 +/- 0.1380	2.39977e+08	18	3.63198e-05	845
pulse-4	13.6865 +/- 0.4576	10.9973 +/- 5.83694	0.6922 +/- 0.1291	8009.32 +/- 214.537	2.8493 +/- 0.6821	0.2429 +/- 0.1894	1.82663e+07	36	1.16843e-08	529
pulse-5	17.7269 +/- 0.1850	0.3442 +/- 0.1834	3.3499 +/- 0.3504	3988.12 +/- 61.2177	5.0607 +/- 0.6915	0.6619 +/- 0.5068	1.60228e+06	39	1.63271e-06	1194

Figure 4.39: Curve-fitting results for 40-142 KeV energy channel

142-524kev	ts	T1	T2	amplitude	Width	asymmetry	Chi-2	NDF	Edm	Ncalls
pulse-1a	-2.6185 +/- 0.2886	112.33 +/- 27.7394	0.1109 +/- 0.0120	20622.6 +/- 269.041	1.2566 +/- 0.1670	0.0883 +/- 0.0719	2.39875e+06	7	3871.9	1485
pulse-1b	0.2779 +/- 0.8751	16.4809 +/- 32.1291	0.0899 +/- 0.0539	28835.2 +/- 2521.33	0.6675 +/- 0.5352	0.1346 +/- 0.1007	1.09923e+08	7	4046.55	1481
pulse-2a	2.2839 +/- 0.0524	0.2141 +/- 0.2094	0.2721 +/- 0.1224	35774 +/- 3547.3	0.5803 +/- 0.3056	0.4689 +/- 0.4006	7.39028e+07	3	1.47244e-07	491
pulse-2b	2.8842 +/- 0.1769	0.0364 +/- 0.1079	2.1153 +/- 2.2401	23320.9 +/- 895.226	2.6117 +/- 3.0699	0.8099 +/- 0.7296	9.69612e+06	4	7.59642e-07	1239
pulse-3a	3.1921 +/- 0.3277	1.5864 +/- 2.3345	0.3176 +/- 0.1511	36754.7 +/- 1853.42	1.0011 +/- 0.6179	0.3171 +/- 0.2445	8.65614e+07	7	1.84513e-06	816
pulse-3b	2.3305 +/- 1.0535	55.2141 +/- 69.0722	0.1059 +/- 0.0544	26730.7 +/- 1876.45	1.0175 +/- 0.6517	0.1041 +/- 0.0835	4.91512e+07	4	11850.8	1481
pulse-3c	1.6182 +/- 0.5801	263.747 +/- 100.591	0.0494 +/- 0.0076	23046.1 +/- 1117.25	0.8464 +/- 0.1632	0.0584 +/- 0.0466	8.11194e+07	18	54952.7	1482
pulse-4	12.4 +/- 0.7613	12.1601 +/- 4.20527	1.3271 +/- 0.1608	1832.22 +/- 72.22	4.8048 +/- 0.7446	0.2762 +/- 0.2159	4.4647e+06	49	115902	1486

Figure 4.40: Curve-fitting results for 142-524 KeV energy channel

524-930kev	ts	T1	T2	amplitude	width	asymmetry	Chi-2	NDF	Edm	Ncalls
pulse-1a	-3.1795 +/- 0.8494	154.95 +/- 72.6944	0.1069 +/- 0.0272	1057.09 +/- 55.1629	1.3238 +/- 0.3918	0.0808 +/- 0.0694	113292	7	143.325	1481
pulse-1b	-0.2694 +/- 0.30834	76.1812 +/- 25.9709	0.0413 +/- 0.0174	2270.65 +/- 383.842	0.5428 +/- 0.2172	0.0761 +/- 0.0802	1.88906e+06	6	1764	1485
pulse-2a	2.1599 +/- 0.0001	1.1864 +/- 0.0001	0.1265 +/- 0.0002	3365.71 +/- 2.0884	1.2080 +/- 0.0008	0.9821 +/- 0.1324	2.29706e+06	6	203187	795
pulse-2b	2.9532 +/- 0.0001	0.0196 +/- 0.0001	0.2843 +/- 0.0002	3717.94 +/- 2.0884	0.4072 +/- 0.0004	0.6981 +/- 0.5110	738022	1	238.846	1484
pulse-2c	3.0103 +/- 0.0007	1.5236 +/- 0.0074	0.11705 +/- 0.0001	2744.04 +/- 0.853302	0.4598 +/- 0.0009	0.2545 +/- 0.1931	1.45952e-08	0	2.93618e-08	1163
pulse-2d	3.2746 +/- 0.2804	1.6032 +/- 2.5208	0.1865 +/- 0.0884	3896.36 +/- 282.613	0.6653 +/- 0.4180	0.2802 +/- 0.2115	2.07626e+06	5	1596.19	148
pulse-3a	4.4754 +/- 0.0639	0.0155 +/- 0.0425	0.6604 +/- 0.3775	1775.14 +/- 368.241	0.8389 +/- 0.5777	0.7872 +/- 0.6535	360779	4	573.351	1490
pulse-3b	3.7922 +/- 0.2981	21.8525 +/- 10.0868	0.0884 +/- 0.0163	1239.25 +/- 83.9084	0.7064 +/- 0.1634	0.1250 +/- 0.0998	185722	8	135.64	1490

Figure 4.41: Curve-fitting results for 524-930 KeV energy channel

4.4.2 Quality of fit

The quality of a fitted curve can be found by the chi-square value divided by the number of degrees of freedom and should be close to 1 but in our case the values came out to be very high or either very low with NDF(number of degrees of freedom) reaching zero at one time indicating a problem with the fit. The fitted curves looked appropriate visually but due to issues with time binning selection or the fact that our chosen model might not be optimum

for this Gamma-Ray Burst can be possible reasons why the goodness of fit values were off. Here Edm is the estimated distance to minimum and Ncalls shows the number of iterations after which convergence occurs. Keeping that in mind we tend to explore this issue in detail, in the future.

5. RELATIONSHIPS AND DISCUSSION

In this chapter we will be discussing the relationships between the pulse parameters calculated using the curve-fitting approach, in the previous chapter and will try to build an understanding of the reasons behind these relationships.

5.1 Pulse Rise and Decay Duration

The two parameters τ_1 and τ_2 are the the two key factors of our chosen model. Exploring these two is very important for our understanding of this model and our GRB. In the figure 5.1 and in figure 5.2 we don't see any clear relation between τ_1 and τ_2 but in figure 5.3, figure 5.4 and in figure 5.5 we see inverse relationship between these two parameters.

This result agrees with the result that [1] got in his research where he explained the reason for this behavior as due to the fact that the two exponential terms in the Norris-2005 model encapsulating τ_1 and τ_2 show two processes happening at once in a Gamma-Ray Burst and both are trying to decrease the affect of each other resulting in the inverse relation. When one process rises the other decreases but both are acting throughout the lifetime of the pulse.

This adds some physical intuition to the GRB mechanics and helps us in getting a deeper insight into what might be happening inside the GRB engine. Thus the two parameters τ_1 and τ_2 prove to be very valuable for our understanding of this GRB.

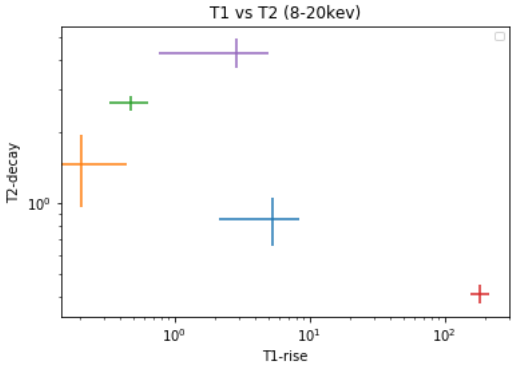

Figure 5.1: Rise and decay timescale relationship for 8-20 KeV

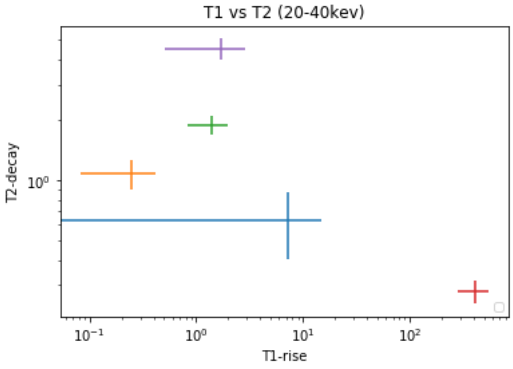

Figure 5.2: Rise and decay timescale relationship for 20-40 KeV

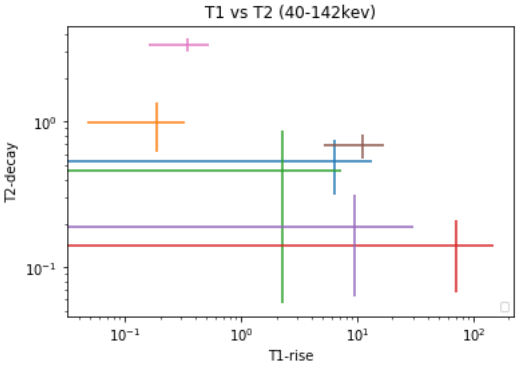

Figure 5.3: Rise and decay timescale relationship for 40-142 KeV

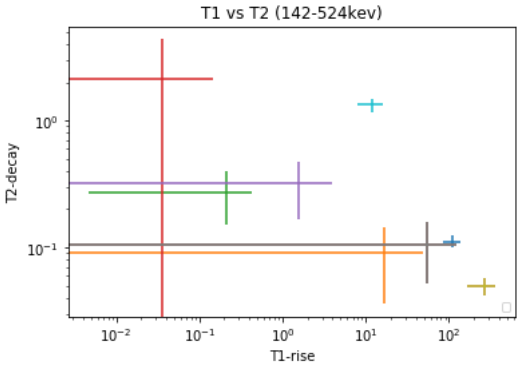

Figure 5.4: Rise and decay timescale relationship for 142-524 KeV

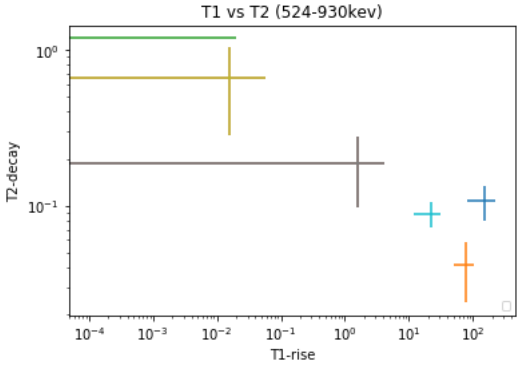

Figure 5.5: Rise and decay timescale relation for 524-930 KeV

5.2 Pulse Width and Asymmetry

The two shape parameters width and asymmetry have been found to have no apparent relationship as seen by figure 5.6, figure 5.7, figure 5.8, figure 5.9 and figure 5.10. Pulse width in the Norris-2005 model is the width between the two exponential terms $\exp\left(-\frac{\tau_1}{t-ts}\right)$ and $\exp\left(-\frac{t-ts}{\tau_2}\right)$. Asymmetry depends on the rise and fall of the pulse and the more unequal they are, the more is the pulse asymmetric. From the formula of asymmetry it might be assumed that there can be an inverse relationship between width and asymmetry but we see graphically that its not true. [1] observed the same results while studying width and asymmetry in long Gamma-Ray Bursts.

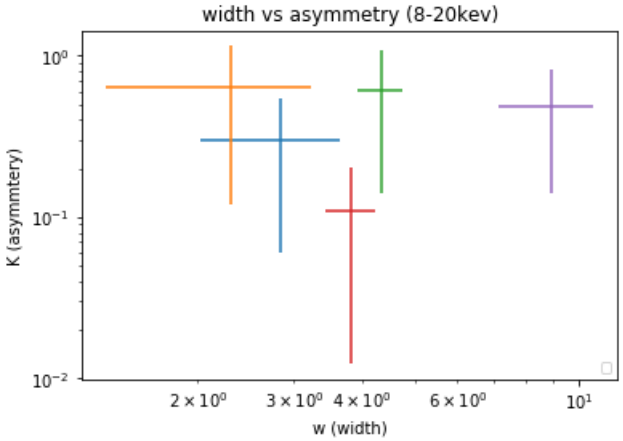

Figure 5.6: Width and asymmetry relation for 8-20 KeV

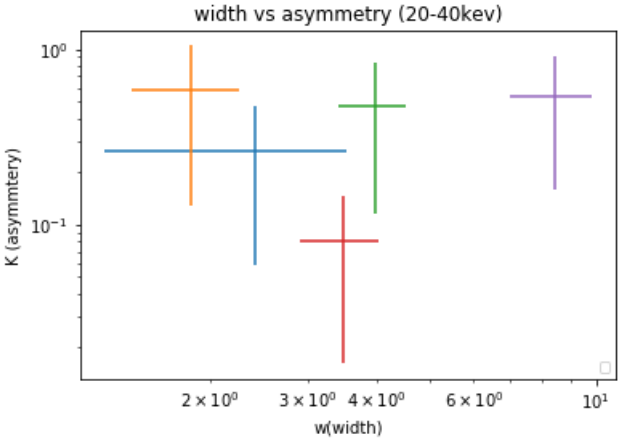

Figure 5.7: Width and asymmetry relation for 20-40 KeV

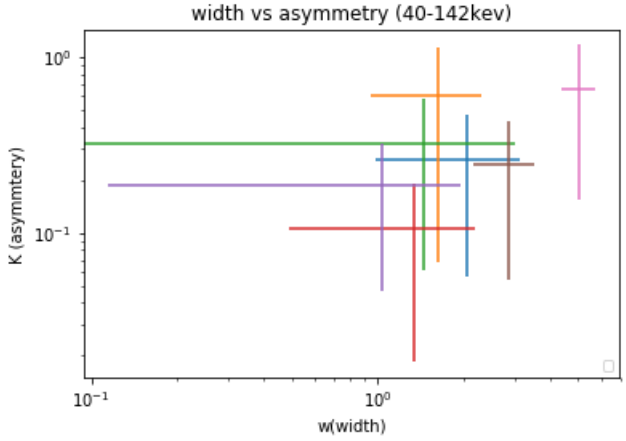

Figure 5.8: Width and asymmetry relation for 40-142 KeV

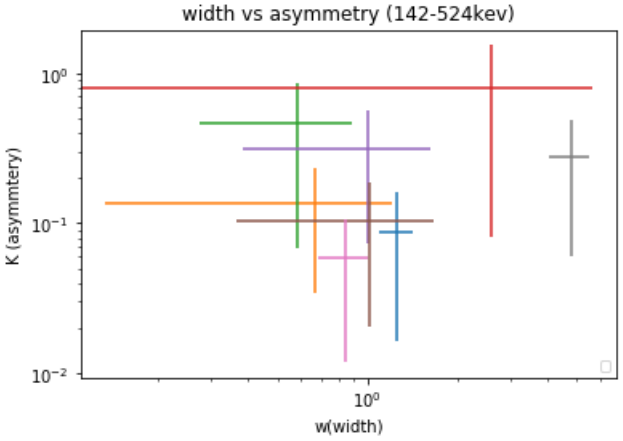

Figure 5.9: Width and asymmetry relation for 142-524 KeV

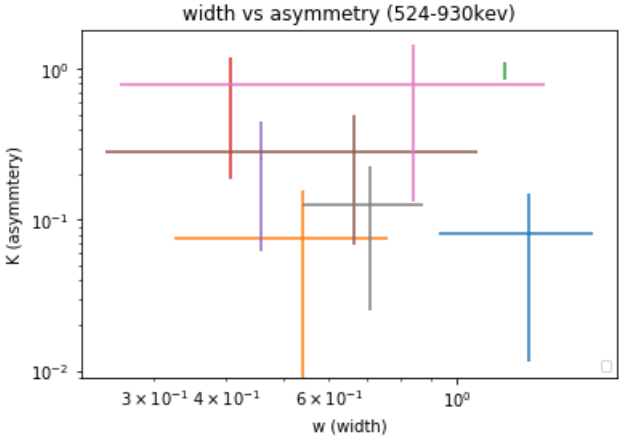

Figure 5.10: Width and asymmetry relation for 524-930 KeV

5.3 Conclusion

We have carried out temporal analysis on the Gamma-Ray Burst 190114C which is a very high energy, long GRB peaking in the Tera-electron Volt energy range. We have performed curve-fitting using the temporal model Norris-2005, Pyroot and background fitting using Rmfit. In the entire energy range of 8 to 930 KeV approx we constructed a light-curve and noticed that the width increased and the amplitude decreased as time passed. While performing curve-fitting in Pyroot using 5 energy channels we found that pulses become narrower in higher energy channels indicating a decrease in width. We also found the highest number of photons in the energy band of 40-142 KeV using the fitted light-curves. Using our curve fitting procedure we calculated the 4 pulse parameters t_s, amplitude, τ_1 and τ_2 given in the Norris-2005 model. Using these results we created plots to relate τ_1 and τ_2 which are the two major parameters of our model and we also related asymmetry and width which are the shape parameters of the Norris-2005 model. The curve-fitting results gave very high chi-2/NDF values indicating an issue with the fit. We also got nan values for some curves which is another concern which can be addressed in future studies.
Looking at our results the GRB 190114C does not show very peculiar behavior as far as the temporal properties are concerned. The rise and fall duration τ_1 and τ_2 show inverse relationship indicating that the processes responsible for them are inversely related to each other. We observed no relationship between width and asymmetry that shows that these two parameters do not affect each other and the processes behind them might be independent.

5.4 Future Directions

We aim to understand the dependence of amplitude, width, τ_1, t_s, asymmetry and τ_2 on energy and to further relate the pulse parameters in order to explore the Norris-2005 model better. By relating all the parameters with each other and their relationship with energy we can enhance our knowledge about GRBs and how much each is related to the other. About our analysis the reason behind the observation of no relationship between width and asymmetry during our analysis isn't apparent but can be explored in the future.

we also aim to work on the GRB 190829A and GRB 180720B which are both long Gamma-Ray Bursts and have energies peaking in TeV (Tera electron-Volt) energy range. We wish to use the log-normal model as well for curve fitting in order to have a practical comparison of the two pulse models. We used one binning of 0.09 seconds but we hope to work with different time binnings in order to explore better curve-fitting scenarios. The Chi-2/NDF values are a major concern for us which we tend to understand further in future studies. The fits looked appropriate visually but very high goodness of fit values and nan values can indicate multiple issues which we hope to explore in detail. During this analysis we found manual selection of binning and entering guess parameters very inconvenient and that made the entire process very slow. An automatic routine might prove useful and may increase the quality of our work greatly thus we hope to explore such methods as well.

Bibliography

[1] J. P. Norris, J. T. Bonnell, D. Kazanas, J. D. Scargle, J. Hakkila, and T. W. Giblin, "Long-lag, wide-pulse gamma-ray bursts," *The Astrophysical Journal*, vol. 627, no. 1, p. 324, 2005.

[2] P. D'Avanzo, "Short gamma-ray bursts: A review," *Journal of High Energy Astrophysics*, vol. 7, pp. 73 – 80, 2015, swift 10 Years of Discovery, a novel approach to Time Domain Astronomy. [Online]. Available: http://www.sciencedirect.com/science/article/pii/S2214404815000415

[3] R. M. Yu Wang, Liang Li and R. Ruffini, "Grb 190114c: An upgraded legend," 2019.

[4] R. Perna, D. Lazzati, and B. Giacomazzo, "Short gamma-ray bursts from the merger of two black holes," *The Astrophysical Journal Letters*, vol. 821, no. 1, p. L18, 2016.

[5] A. Pe'er, "Physics of gamma-ray bursts prompt emission," *Advances in Astronomy*, vol. 2015, p. 1–37, 2015. [Online]. Available: http://dx.doi.org/10.1155/2015/907321

[6] D. Bégué and J. M. Burgess, "The anatomy of a long gamma-ray burst: A simple classification scheme for the emission mechanisms," *The Astrophysical Journal*, vol. 820, no. 1, p. 68, Mar 2016. [Online]. Available: http://dx.doi.org/10.3847/0004-637X/820/1/68

[7] J. Norris, R. Nemiroff, J. Bonnell, J. Scargle, C. Kouveliotou, W. Paciesas, C. Meegan, and G. Fishman, "Attributes of pulses in long bright gamma-ray bursts," *The Astrophysical Journal*, vol. 459, p. 393, 1996.

[8] G. J. Fishman, "Gamma-ray bursts: An overview," *Publications of the Astronomical Society of the Pacific*, vol. 107, no. 718, p. 1145, 1995.

[9] F. Quilligan, B. McBreen, L. Hanlon, S. McBreen, K. Hurley, and D. Watson, "Temporal properties of gamma ray bursts as signatures of jets from the central engine," *Astronomy & Astrophysics*, vol. 385, no. 2, pp. 377–398, 2002.

[10] Z. Zhang and G. Xie, "A comparison of temporal properties of short and long gamma-ray bursts," *Astrophysics and Space Science*, vol. 310, no. 1-2, pp. 19–23, 2007.

[11] T. Yi, E. Liang, Y. Qin, and R. Lu, "On the spectral lags of the short gamma-ray bursts," *Monthly Notices of the Royal Astronomical Society*, vol. 367, no. 4, pp. 1751–1756, 03 2006. [Online]. Available: https://doi.org/10.1111/j.1365-2966.2006.10083.x

[12] J. Hakkila, T. W. Giblin, J. P. Norris, P. C. Fragile, and J. T. Bonnell, "Correlations between lag, luminosity, and duration in gamma-ray burst pulses," *The Astrophysical Journal*, vol. 677, no. 2, pp. L81–L84, mar 2008. [Online]. Available: https://doi.org/10.1086%2F588094

[13] Z. Peng, Y. Yin, T. Yi, Y. Bao, and H. Wu, "A comprehensive comparative study of temporal properties between x-ray flares and grb pulses," *Astrophysics and Space Science*, vol. 355, no. 1, pp. 95–103, 2015.

[14] Z. Y. Peng, Y. Yin, X. W. Bi, X. H. Zhao, L. M. Fang, Y. Y. Bao, and L. Ma, "The Temporal and spectral characteristics of "fast rise and exponential decay" Gamma-Ray Bursts pulses," *The Astrophysical Journal*, vol. 718, no. 2, pp. 894–898, jul 2010. [Online]. Available: https://doi.org/10.1088%2F0004-637x%2F718%2F2%2F894

[15] Yassine, M., Piron, F., Mochkovitch, R., and Daigne, F., "Time evolution of the spectral break in the high-energy extra component of grb 090926a," *A&A*, vol. 606, p. A93, 2017. [Online]. Available: https://doi.org/10.1051/0004-6361/201630353

[16] J. Hakkila and R. D. Preece, "Unification of pulses in long and short Gamma-Ray Bursts: evidence from pulse properties and their correlations," *The Astrophysical Journal*, vol. 740, no. 2, p. 104, oct 2011. [Online]. Available: https://doi.org/10.1088%2F0004-637x%2F740%2F2%2F104

[17] R. Shen and L. Song, "Characteristic variability time scales of long gamma-ray bursts," *Publications of the Astronomical Society of Japan*, vol. 55, 02 2003.

[18] P. N. Bhat, M. S. Briggs, V. Connaughton, C. Kouveliotou, A. J. van der Horst, W. Paciesas, C. A. Meegan, E. Bissaldi, M. Burgess, V. Chaplin, R. Diehl, G. Fishman, G. Fitzpatrick, S. Foley, M. Gibby, M. M. Giles, A. Goldstein, J. Greiner, D. Gruber, S. Guiriec, A. von Kienlin, M. Kippen, S. McBreen, R. Preece, A. Rau, D. Tierney, and C. Wilson-Hodge, "Temporal deconvolution study of long and short Gamma-Ray Bursts light-curves," *The Astrophysical Journal*, vol. 744, no. 2, p. 141, dec 2011. [Online]. Available: https://doi.org/10.1088%2F0004-637x%2F744%2F2%2F141

[19] S. NuSTAR, "Rapid variability of blazars 3c 279 during flaring states in 2013-2014 with joint fermi-lat," *arXiv preprint arXiv:1502.04699*, 2015.